# MESOSCOPIC AND MICROSCOPIC ANALYSES OF ROCK SAMPLES UTILIZED IN ROCK MECHANICS STUDIES

1986 Annual Report

By M. P. R. Light

Prepared for the
U.S. Department of Energy
Division of Geothermal Energy
under Contract No. DE-FC07-85NV10412

Bureau of Economic Geology
W. L. Fisher, Director
The University of Texas at Austin
Austin, Texas 78713

June 1987

## DISCLAIMER

CONTENTS

Figures

Tables

# ABSTRACT

Uncompacted and experimentally compacted rock samples from Frio 'A' sandstones and Anahuac shales, Hitchcock N.E. field (Galveston County), utilized in rock mechanics studies were investigated mesoscopically and microscopically to determine fabric and grain movement. Sandstone petrography and porosity reduction were measured by point counting to estimate the degree of shortening the sandstones had undergone. Rounded, irregular to elongate grains of quartz, feldspar, rock fragments, chlorite and shale clasts, and cements form the main constituents of the Frio 'A' reservoir. Quartz and feldspars are corroded, whereas skeletal and vacuolized feldspars form about 2 percent of the sandstones.

The Frio 'A' reservoir consists of a stacked sequence of distributary-mouth-bar sandstones, delta plain units, and delta destructional units overlain by the transgressive Anahuac shale. Grains within these sandstones are imbricated in shallow to steeply dipping crossbeds. Steeply dipping interference banding present on Fry (1979) diagrams constructed from grain distributions in mouth-bar sandstones result from foreset bedding.

Point count analyses indicate that the porosity has been reduced by 42 to 62 percent during experimental compaction. Collapse of skeletal and vacuolized feldspars would reduce measured porosities by 7 to 10 percent, whereas some additional compaction can be taken up by deformation of ductile grains. A linear relationship exists between percent porosity reduction and content of ductile grains and cements in the Frio 'A' sandstones. These grains and cements have deformed and lubricated grain margins and thus facilitated intergranular rotation and movement, allowing greater shortening to occur where they are more abundant.

Experimental compaction has resulted in the development of vertical extension fractures and shears inclined at 16 to 45 degrees to the direction of maximum vertical stress. A shear fracture in a friable mouth-bar sandstone at 9,166 ft (2,794 m) is rimmed by a 3- to 5-mm-wide zone, within which the rock has almost retained its original precompaction porosity. Horizontal and irregular vertical expansion fractures have formed simultaneously during post-compaction decompression of cores.

During experimental compaction, steeply imbricated elongated grains have rotated more than 30 degrees into shear and vertical extension fractures that have facilitated movement of grains through bedding into vacant pore spaces to produce a closely packed structure. More shallowly imbricated elongated grains have rotated toward bedding. This rotation and intergranular movement appear to be the major deformation the Frio 'A' sandstones have undergone during experimental compaction.

Initial strain ellipses in Fry (1979) diagrams represent the preferred direction of grain orientation, porosity development, and fluid-flow direction in the Frio 'A' sandstones. Experimental compaction has changed the axial ratios of initial strain ellipses by 10 to 77 percent. After compaction, the trend of strain ellipse remains parallel to the imbricate direction in the clean mouth-bar sandstones preserving the interbed flow characteristics of these rocks. However, the strain ellipse has been rotated into bedding in the clean channel sandstones, which show greatly reduced porosities from compaction. Interbed porosity is thus greatly reduced by compaction in the distributary channel sandstones.

Development of crosscutting compaction shears in the clean distributary-mouth-bar sandstones surrounded by a 3- to 5-mm-wide zone in which the pre-compaction porosity is largely retained has implications for the maintenance of large production rates in geopressured and coproduction reservoirs. These compaction fractures may

preferentially open during hydraulic fracturing of the compacted sandstones and form excellent conduits for increased fluid flow to the well bore.

Knowledge of the preferential fluid-flow directions in sandstone reservoirs is critical in efficiently locating production boreholes in geopressured and hydrocarbon reservoirs and guard wells in coproduction fields.

## INTRODUCTION

Mesoscopic and microscopic analyses of rock samples utilized in rock mechanics studies were originally designed to determine the fabric and movement history (Turner and Weiss, 1963) of undeformed and experimentally deformed Frio 'A' reservoir sandstones from the Hitchcock N.E. field (Galveston County, Texas). These Upper Frio sandstones were deposited in the same distributary-mouth-bar environment as the Lower Frio "Andrau" geopressured sandstones at the Pleasant Bayou well, and their fabrics and movement history under experimental deformation should therefore be similar. The fabric and movement of undeformed and experimentally deformed deltaic sandstones were to be determined by mesoscopic, transmission, and scanning electron microscopic (SEM) analyses of oriented core samples. The preferred orientation of mineral grains was to be measured using a universal stage. This project was designed to complement the detailed rock mechanics studies being conducted at The University of Texas at Austin.

Because of a cutback in funding for this project and the presence of a very mixed and deformed initial mineralogy in the Frio 'A' sandstones, it was decided to discontinue universal stage work and to apply Fry's (1979) method of graphical fabric analysis. Fry's (1979) method, which employs microphotography and is computerized, is considerably faster than the universal stage method and would allow a more complete analysis within the limited time available. Eighteen rock sections were also

point counted to measure the reduction in porosity and thus degree of shortening the sandstones had undergone as a result of experimental compaction.

The Frio 'A' sandstones were found to contain abundant rounded, angular, and elongated quartz and feldspars showing a varied assemblage of deformation textures and undulose extinction, which made the use of the universal stage as a grain-orienting mechanism unsatisfactory. Furthermore, there were abundant elongated rock fragments whose orientation could not be measured by the universal stage method. The Fry (1979) method, which considers only the relative position of grain centers, and the overlay (grain long axis) method take account only of grain position and shape and are therefore more reliable indicators for detecting changes in grain fabric due to experimental compaction.

Ragan (1968) has outlined the relationship between imposed triaxial stresses and subsequent strains resulting from them in deformed rocks. Stress at any point can be represented by three mutually perpendicular stresses; the greatest principal stress (sigma 1), the intermediate principal stress (sigma 2), and the least principal stress (sigma 3) (fig. 1a). Only planes parallel to the principal (vertical) stress (sigma 1) are subjected solely to normal stress, whereas on all other planes stress includes a normal stress intermediate between sigma 1 and sigma 3 and a shearing stress (Tau) acting parallel to the plane (fig. 1b). When brittle or semibrittle isotropic rocks fail under compression, two conjugate sets of fractures may form (fig. 1c), usually at angles (of internal friction) of 30 to 45 degrees to the greatest principal (vertical) stress sigma 1.

Where rocks have undergone homogeneous strain as a result of imposed stresses, spheres become ellipsoids, circles become ellipses, and lines and planes become linear and planar (Ragan, 1968). In normal strain, both distortions and rotations occur

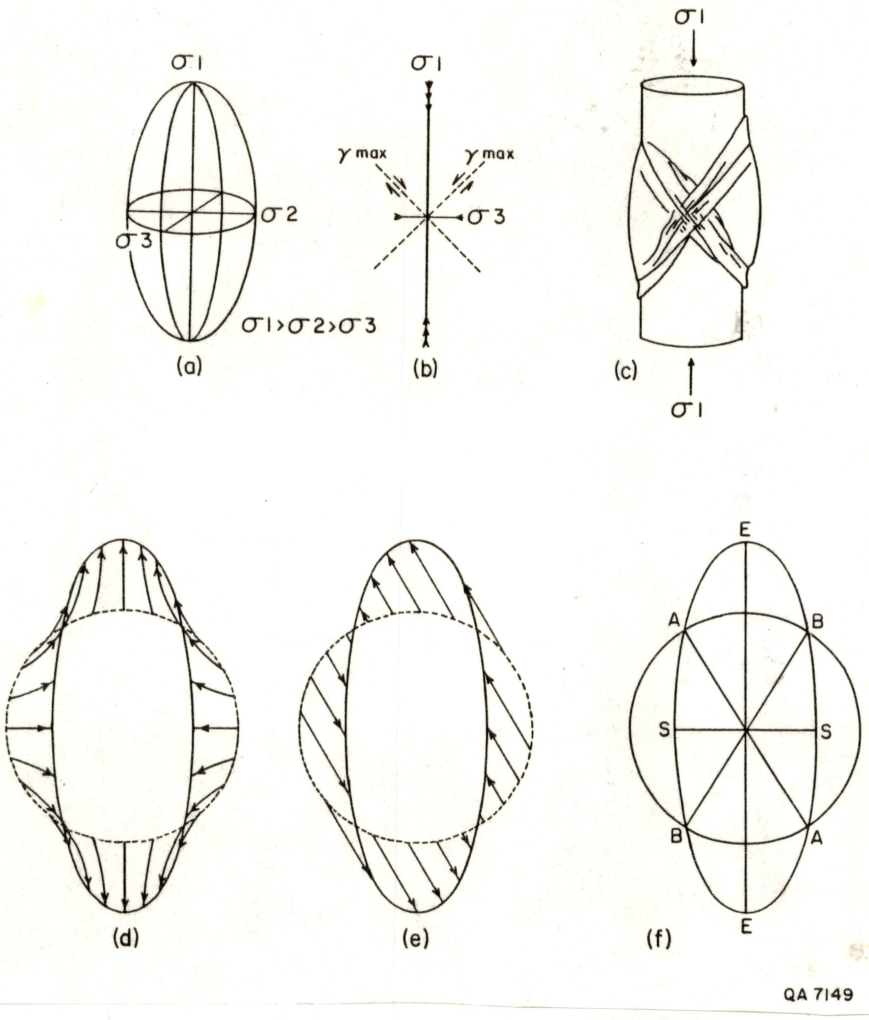


Figure 1. (1a) Geometry of triaxial stresses. (1b) Plane showing traces of planes of maximum shearing stress (Tmax) and conjugate fractures in experimentally deformed rock cylinder showing semibrittle behavior. (1c) Different movement patterns that produce identical strain ellipses. (1d) Pure shear. (1e) Simple shear. (1f) Relationship between initial circle, strain ellipse, and lines of no finite longitudinal strain (A-A) and (B-B). Figures after Ragan, 1968.

though only the irrotational component is considered in strain analysis and the volume is assumed to be constant. However, in clastic rocks with a high porosity this constant volume assumption is invalid, as shown by the large reduction in porosity of the Frio 'A' sandstones after experimental compaction (tables 1 and 2).

Different types of movement patterns such as pure and simple shear can also produce identical strain ellipses (fig. 1d and 1e). During homogeneous strain (volume constant) all lines in a material are elongated or shortened (fig. 1d and 1e). The lines of maximum (E-E) and minimum (S-S) elongation of an ellipse (fig. 1f) are termed the principal strains, and their orientation and values define the irrotational strain component. The relative change in the elongation can be defined by the reciprocal quadratic elongation:

$$\text{Lambda} = L0^2/L1^2$$

Where L0 = original length

L1 = new length

(Ragan, 1968).

The Fry (1979) method has been used to produce strain ellipses in both the uncompacted and the experimentally compacted sandstones, but as strain has involved a major volume change only the relative elongation has been estimated.

Fry's simple and elegant method for determining the finite strain in a rock (Fry, 1979: Hanna and Fry, 1979), being relatively rapid and practical, is suited to rocks that lack plastically deformed elliptical markers (Crespi, 1986). A central vacancy field in the Fry (1979) diagram shows a very low point concentration, which can have a circular (no strain) or elliptical (rock subjected to strain) form (Ramsay and Huber, 1983). The shape and orientation of the strain ellipse are directly recorded by the

Table 1. Point count analyses of 18 Frio 'A' sandstone samples, Delee No. 1 well.

| Sample No. | Depth of Core Samples | Porosity % | Brittle Grains % | Ductile Grains % | Shale and Carbonate Cement % | Number of Points Counted | State of Core |
|---|---|---|---|---|---|---|---|
| 09001 | 9156.06 | 13.51 | 64.87 | 15.67 | 5.95 | 185 | Uncompacted |
| 09000 | 9156.06 | 15.25 | 50.75 | 15.0 | 19.0 | 200 | Uncompacted |
| 09012 | 9156.06 | 7.25 | 71.25 | 11.0 | 10.5 | 200 | Compacted |
| 09013 | 9156.06 | 5.3 | 65.37 | 19.23 | 10.1 | 208 | Compacted |
| 09015 | 9156.06 | 7.0 | 65.75 | 16.25 | 11.0 | 200 | Compacted |
| 09003 | 9166.0 | 18.5 | 70 | 6.75 | 4.75 | 200 | Uncompacted |
| 09004 | 9166.0 | 22.7 | 63.76 | 7.14 | 6.4 | 203 | Uncompacted |
| 09017 | 9166.0 | 11.03 | 71.6 | 10.09 | 7.28 | 213 | Core Center Compacted |
| 09017 | 9166.0 | 19.38 | 64.33 | 9.83 | 6.46 | 178 | Shear Area Compacted |
| 09018 | 9166.0 | 12.79 | 76.75 | 7.44 | 3.02 | 215 | Compacted |
| 09006 | 9178.3 | 16.5 | 63.5 | 16.75 | 3.25 | 200 | Uncompacted |
| 09007 | 9178.3 | 18.5 | 64.25 | 13.5 | 3.75 | 200 | Uncompacted |
| 09021 | 9177.5 | 8.53 | 69.73 | 20.52 | 1.22 | 246 | Compacted |
| 09020 | 9177.5 | 11.19 | 56.08 | 29.5 | 3.23 | 201 | Compacted |
| 09009 | 9189.5 | 21.7 | 61.23 | 12.68 | 4.39 | 205 | Uncompacted |
| 09010 | 9189.5 | 17.75 | 62.75 | 15.5 | 4.0 | 200 | Uncompacted |
| 09025 | 9189.5 | 6.76 | 68.16 | 15.42 | 9.66 | 207 | Compacted |
| 09026 | 9189.5 | 8.5 | 63.75 | 22 | 5.75 | 200 | Compacted |

Table 2. Averaged point count analyses of Frio 'A' sandstone samples, Delee No. 1 well.

| Depth of Core Samples | Porosity % | Brittle Grains % | Ductile Grains % | Shale and Carbonate Cement % | Ductile Grains and Carbonate Cement % | Number of Points Counted | Total Shortening | % Porosity Reduction per unit Porosity | Normalized % Porosity Reduction |
|---|---|---|---|---|---|---|---|---|---|
| 9156.06 | 14.4 | 59.2 | 15.5 | 10.9 | 26.4 | 993 | 7.9 | 54.7 | 55.7 |
| 9166 | 20.6 | 66.3 | 7.8 | 5.3 | 13.1 | 1,009 | 8.7 | 42.2 | 38.8 |
| 9177.5 | | | | | | | | | |
| 9178.3 | 17.5 | 63.8 | 16.0 | 2.7 | 18.7 | 847 | 7.6 | 43.7 | 45.7 |
| 9189.5 | 19.8 | 61.8 | 15.2 | 3.25 | 18.5 | 812 | 12.1 | 61.3 | 40.5 |

elliptical form of the field, and if no vacancy field exists after 50 moves of the grain centers, the initial aggregate is inferred to possess a completely random arrangement (Ramsay and Huber, 1983). Under these circumstances no final solution can be found (Ramsay and Huber, 1979).

An additional problem is the existence of an initial eccentricity of grains prior to straining, as the deformed shape of grains does not directly reflect the shape of the strain ellipsoid (Lisle, 1979). Their final axial ratios and orientations are a result of the combined effects of their pre-tectonic (sedimentary) elongations (axial ratios) and the superimposed strain (Lisle, 1979). Furthermore, elliptical vacancy fields in some the Fry (1979) diagrams from Frio 'A' sandstones have been reduced to circular vacancy fields during the experimental compaction, which makes the direct use of the strain ellipse as an indicator of strain questionable.

Fry's (1979) method requires the distribution of the strain markers to be anticlustered as opposed to random (Crespi, 1986). An anticlustered distribution has a preferred minimum distance between points such as a hexagonal grid of points (Fry, 1979). In a random (Poisson) distribution, there are no constraints in positioning the points, and the minimum allowable distance is zero (Crespi, 1986). Fry (1979) noted that the closer a distribution departs from a random distribution toward an anticlustered the greater the accuracy in the determination of the strain ellipse. The degree of anticlustering is a function of several variables but tends to be equated directly with sorting (Bhattacharya and Longiaru, 1986; Onasch, 1986a,b).

Fry (1979) diagrams are characterized by a central vacancy field that may have a girdle of high point density for strongly anticlustered distributions (Crespi, 1986). In order to perfectly define the strain ellipse at least 50 points are required bounding the

vacancy field, which necessitates the use of 100 contiguous grain centers in a strongly anticlustered distribution and more than 800 points for weakly anticlustered distributions (Crespi, 1986).

Strongly to very strongly anticlustered distributions have degrees of anticlustering between 0.73 and 0.86 (Crespi, 1986). Poorly sorted graywackes (Rousel, 1972) and well-sorted sandstones (Wanless and others, 1955) have degrees of anticlustering of 0.66 and 0.70, respectively (Crespi, 1986). Frio 'A' sandstones are on average moderately sorted and would thus have a degree of anticlustering near 0.68. This implies that some 200 grain centers would need to be used to generate a perfect strain ellipse on the Fry (1979) diagrams (Crespi, 1986). This is in contrast to the relatively small number of contiguous grain centers (50) that Ramsay and Huber (1983) state are required to determine the shape of the vacancy field.

More than 200 grain centers were used in initial tests of the Fry (1979) diagrams for Frio 'A' sandstones at 9,166 ft (2,794 m). However, these diagrams took up to 30 minutes to run, and the point density usually masked out any interference patterns visible in the surrounding fields in diagrams constructed with fewer points. Fifty grain distributions were also found to generate ellipse-shaped vacancy fields more closely related to grain shape and orientation. Furthermore, the use of the strain ellipsoid to determine imposed deformational strain assumes no volume change (Ragan, 1968), which is invalid for the Frio 'A' experimentally deformed sandstones. Two sets of Fry (1979) diagrams with around 200 and 50 grain centers were generated in order to determine qualitative changes in the rock fabric from experimental compaction.

Onasch (1986a,b) modeled pressure-solution deformation using the Fry (1979) method and concluded that the Fry (1979) diagram for pressure-solution deformation would be characterized by vertical zones of high point density corresponding to

dissolution surfaces and have a poorly defined central vacancy with little bearing on the total strain in the model. Very few stylolitic contacts were observed in the Frio 'A' sandstones, although quartz overgrowths do occur and pressure-solution deformation appears to be of minor importance in the experimental compaction of these sandstones.

## FACIES ANALYSIS AND DEPOSITIONAL ENVIRONMENT

### General Depositional Environment

The general depositional environment of the Frio 'A' sandstone in the area of the Hitchcock N.E. field has been described by Light (1985). This gas-condensate reservoir consists of a stacked sequence of distributary-mouth-bar sandstones and thin delta plain and destructional units and is overlain by the transgressive Anahuac shale.

A light-gray, fine to medium grained, moderately sorted sandstone occurs near the base of the Frio 'A' interval at 9,189.5 ft (2,801 m). This well-bedded sandstone is highly indurated, contains spotty kaolinite cement, and is moderately contorted. Irregular layers of calcareous material occur within it, especially near the top where an upper channel unit has erosively cut into the basal sandstones. Sedimentary structures such as plane bedding and penecontemporaneous slumps suggest upper-flow-regime sedimentation conditions and high pore pressures, respectively. These structures imply rapid deposition of the sand body (Coleman and Prior, 1980). The indurated sandstone at 9,189.5 ft (2,801 m) is cross-bedded and upward fining and is interlayered with planolites bearing rippled marine shales, suggesting that it is a distributary channel.

A very uniform, fine- to medium-grained, cross bedded, glauconitic sandstone forms a 24 ft (7.3 m) thick porous interval from 9,157 ft (2,791 m) to (2,798 m) where it has a sharp contact with underlying shales. These even grained sandstones are light green, light gray-green, and tan and contain clear to milky quartz grains. The rounded quartz grains appear to be coated with iron oxide, suggesting a fluvial derivation (N. Tyler, personal communication, 1985), whereas inclined and horizontal burrows and contorted bedding imply periods of rapid deposition (Blatt and others, 1972; Reineck and Singh, 1975). The upward decrease in porosity and permeability and presence of carbonaceous material, mica, and glauconite suggest deposition in a fluvially dominated mouth-bar deposit (Selley, 1979; Coleman and Prior, 1980). Near the base of the 24-ft (7.3 m)-thick interval at 9,177.5 ft and 9,178.3 ft (2,797.3 m and 2,797.6 m) the crossbedded mouth-bar sandstones are very indurated and contain spotty patches of authigenic kaolinite cement that have reduced reservoir quality (Light and D'Attilio, 1985). The upper half of the 24-ft-thick (7.3 m) sandstone unit (9,157 ft to 9,167 ft; 2,791 m to 2,794 m) is burrowed at various levels, more variable in nature, more closely laminated, and shows indistinct bedding.

The major distributary-mouth-bar unit is capped by a thin, upward-fining channel sandstone (9,156 ft to 9153.5 ft; 2,791 m to 2,790 m) that is erosively based and contains a lag conglomerate. These fine- to medium-grained, moderately sorted cross-bedded sandstones are light-green to tan. The channel sandstone is indurated and very calcareous at the base but grades up into fine sandstones interbedded with silty shales near the top. The subrounded and moderately sorted initial fabric of the channel sandstone is similar to that of the underlying stacked distributary mouth bar, suggesting that it has cut its way through its own distributary-mouth-bar system.

## Initial Clastic Fabrics

The degree of preferred orientation in coastal sandstones is strongly affected by local morphology, wave energy, ripple formation, biogenic activity, penecontemporaneous deformation, and post-depositional effects (Seibold, 1963). Sand-grain orientation is more sensitive than other sedimentary structures (e.g., pebble orientation) in providing information on local details and variations of fluid flow (fig. 2) (Reineck and Singh, 1975). Quartz grains tend to be oriented perpendicular to the elongation of coastal sand bodies, whereas fluvial sand grains lie parallel to the elongation of the sand body (Wendler, 1956; Young and Mankin, 1961; Reineck and Singh, 1975). Sand-grain elongation in sand bodies of known origin can be used to define the configuration of the sand body (Curray, 1956), whereas the origin of a sand body can be predicted if the orientation of the sand grains and configuration of the sand body are known (Reineck and Singh, 1975).

On beaches, quartz grain orientation is mainly controlled by the direction of backwash (ebb-flow) and wave propagation parallel to which the grains are oriented (Nanz, 1955; Curray, 1956; Spriramadas, 1957). Nachtigall (1962) and Seibold (1963) found that quartz grains in coastal sands also show a subordinate maximum normal to current flow while in certain cases they may be faintly imbricated (Rusnak, 1957).

The average fabric direction in foresets is similar to the trend of the parting lineation and hence current direction (fig. 2)(Potter and Mast, 1963). Quartz grains are imbricated upcurrent on foresets and where sand has been heaped underwater to produce a monoclinic symmetry (fig. 3)(Schwarzacher, 1951; McBride, 1960; Potter and Mast, 1963).

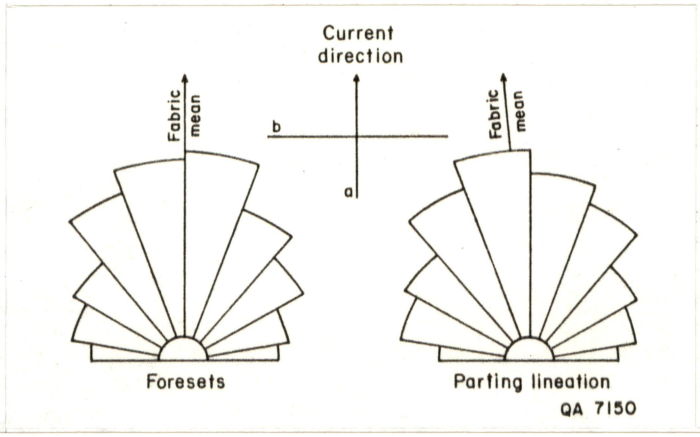


Figure 2. Relationships between current direction and apparent long axes of 3,493 quartz grains from foreset beds and 1,102 quartz grains from parting lineation. Average direction of long axis is closely parallel to current direction as defined by current structures. After Potter and Mast, 1963.

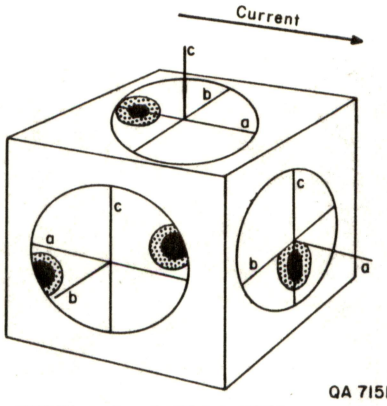


Figure 3. Block diagram of homogeneously anisotropic sandstone in which the long axis orientation and imbrication of sand-sized particles display a monoclinic symmetry. After Potter and Mast, 1963.

## MESOSCOPIC AND MICROSCOPIC ANALYSES

### Fracture Systems

Experimentally compacted Anahuac shale and Frio 'A' sandstone cores were subjected to mesoscopic structural analysis with a binocular microscope and photographed prior to rock sectioning. Several intersecting fracture systems were observed.

A compacted glauconitic siltstone core at 9,068.3 ft (2,764 m) within the Anahuac Formation shows a well-developed listric shear fracture dipping at 30 degrees, along which glauconite grains have become iron stained. This core is also cut by an en echelon set of subhorizontal extension fractures that dip at 10 to 12 degrees and splay out adjacent to the cross-cutting shear fracture. No iron-stained glauconites occur along the extension fractures, indicating that they postdate the shear formation.

At 9,072.8 ft (2,765 m) a compacted Anahuac shale core contains swarms of en echelon and sigmoidal splay fractures formed adjacent to oblique shears, suggesting that shearing is a more penetrative phenomenon in this rock. A compacted Anahuac shale core at 9,076 ft (2,766 m) contains a listric shear which has a decreasing dip angle from 84 degrees at the top to 45 degrees near the base. Slickensides present on the shear plane make an angle of 38 degrees with the vertical, indicating that shearing was subvertical. The listric shear displaces straight to irregular horizontal extension fractures that have different and often opposite displacements on either side of the shear, indicating that they postdate shearing.

A horizontal extension fracture is terminated by the shallowly dipping base of a shear fracture in the compacted Anahuac shale core at 9,081.1 ft (2,768 m). This shear fracture predates the extension fracture but has been reactivated as an extension fracture during decompaction. Similarly in a compacted Anahuac shale core at

9,067.3 ft (2,764 m) (fig. 4) horizontal extension fractures are displaced by well-developed, fairly straight vertical extension fractures. These horizontal extension fractures have different and often opposite displacements on opposite sides of the vertical fracture, indicating that they formed after it.

Other vertical extension fractures in the Anahuac shale core at 9,067.3 ft (2,764 m), which are too irregular (fig. 4) for vertical displacement to have occurred along them, displace some horizontal extension fractures while they terminate against others, suggesting that they formed at a similar time.

During the phase of experimental compaction and vertical rock shortening, shear fractures formed, and high-temperature oxidizing fluids resulted in oxidization of glauconites along these shears in glauconitic siltstones. Shear formation has been more penetrative and resulted in the deformation of a wide zone in the shales. Relatively straight vertical extension fractures (parallel to maximum stress) may have formed simultaneously with the shear fractures or later in the more shaly rocks. Evidently decompression of the shale cores following experimental compaction has resulted in the almost simultaneous development of irregular vertical and subhorizontal extension (expansion) fracture systems. The horizontal breaks have been controlled by weak bedding contacts, which have allowed them to jump to different levels on either side of the vertical extension fractures.

Three sets of fracture systems have developed in the experimentally compacted crossbedded channel sandstone at 9,156 ft (2,791 m)(fig. 5). An open, in part en echelon, subvertical extension fracture dipping at 72 degrees appears to be an intergranular (fig. 5a) break and has formed from relative stress release during experimental compaction. Muscovite mica flakes were seen to extend into the open fracture and were not deformed, indicating that no shearing occurred during the opening of this fracture set. Small shear fractures have formed on either side of the


Figure 4. Experimentally compacted Anahuac shale core (9,067.3 ft, 2,764 m) showing (4a), development of vertical and horizontal extension fractures as well as (4b), irregular vertical fracture systems.

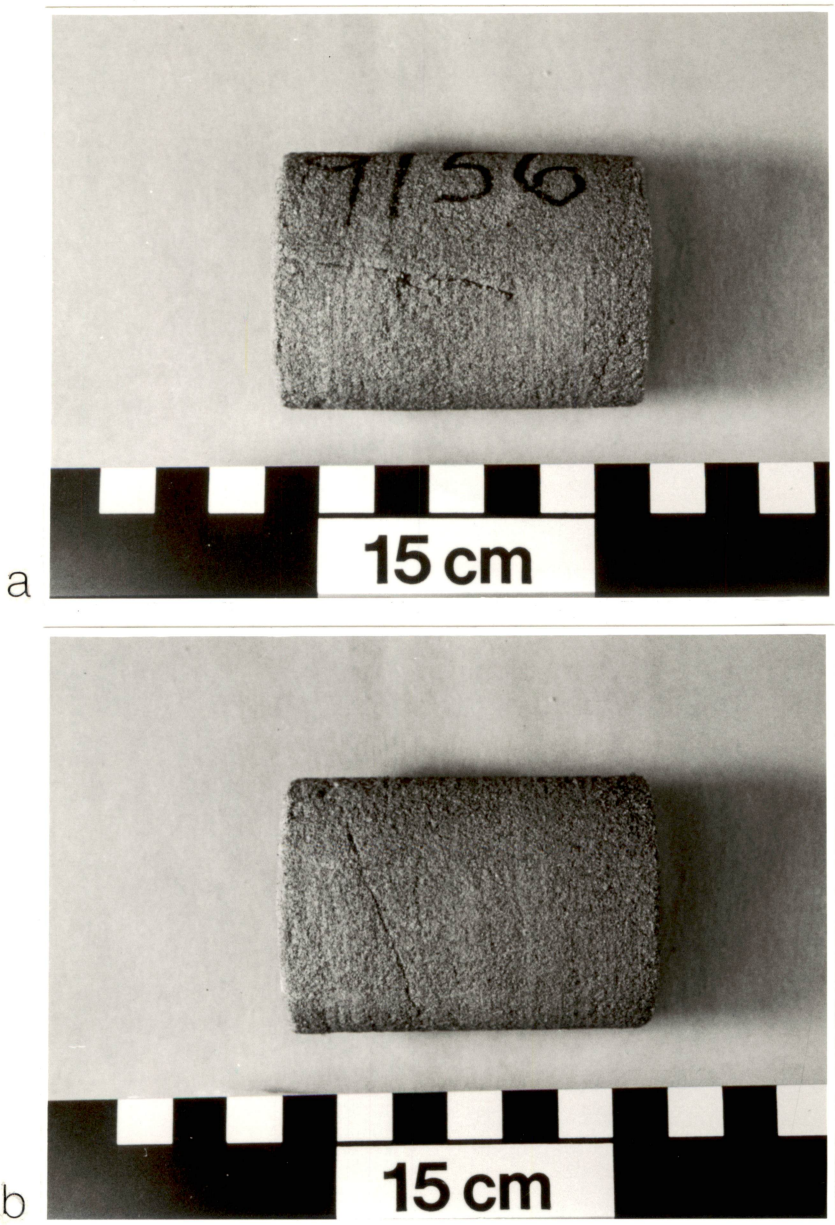


Figure 5. Experimentally compacted Frio 'A' sandstone core (9,156 ft, 2,791 m) showing development of (5a), steep, and (5b), shallowly dipping fractures.

subvertical extension fracture inclined at angles of 24 to 33 degrees to it. The shear fractures postdate the extension fracture as they terminate against it.

An open extension fracture dipping at 27 degrees (fig. 5b) has developed along one of the brownish (iron-carbonate-rich) crossbed lamina that occur erratically within this rock. This fracture is intergranular and has apparently opened during stress release at the termination of the compaction experiment.

## Diagenetic Textures of Channel Sandstones

Microscopic analyses of the channel sandstone at 9,156 ft (2,791 m) indicate that it is very poorly sorted, containing rounded, angular to elongate grains of quartz, feldspar (plagioclase, orthoclase and microcline, and microcline perthite), chert, volcanic, igneous, and metamorphic rock fragments, chlorite and shale clasts, and accessory hyperthenes, garnets, and ores. Quartz and feldspars are corroded, and skeletal and vacuolized feldspars formed during secondary porosity development are abundant.

Kaolinite that postdates quartz corrosion has replaced feldspars. Quartz overgrowths are present, whereas the feldspars are sericitized. Plagioclase shows alteration to sericite along cleavages and is rimmed by later kaolinite, whereas late-stage chlorite cement crosscuts kaolinite intergrowths. Dark-reddish-brown iron carbonate with some sparry calcite cements crosses beds that show increased concentrations of chlorite clasts and volcanic rock fragments. The iron carbonate cement has partly formed from the breakdown of feldspar that it sometimes rims. Sparry calcite also rims corroded feldspars. Detrital biotites, muscovites, and chlorites occur sparingly.

Very little penetrative deformation is visible in the channel sandstone at 9,156 ft (2,791 m). Deformation bands are present in irregular K feldspars, and some appear to be oriented at angles of 30 to 40 degrees to the direction of maximum stress. The deformation bands are displaced in one crystal by a short shear oriented at 45

degrees to the principal direction of stress. One muscovite flake oriented at 45 degrees to the direction of maximum stress showed slight kinking, and deformation twins in an adjacent plagioclase were oriented parallel to the axis of the kink.

Two fracture sets are present in the experimentally compacted channel sandstone at 9,189.5 ft (2,801 m). An early, fairly irregular shear fracture dips at 66 to 69 degrees and is refracted through kaolinite and calcareous cemented beds (fig. 6a). Late horizontal extension fractures occur at the one end of the core and crosscut the shear fracture. The development of intergranular rock flour, which postdates original coring and mudstaining of the rock, suggests that shearing has rotated and comminuted grains.

The channel sandstone at 9,189.5 ft (2,801 m) contains the same mineral assemblage as that described in the channel sandstone at 9,156 ft (2,791 m). However, only a trace of reddish-brown iron calcite and sparry calcite cement occurs in the channel sand at 9,189.5 ft (2,801 m), whereas kaolinite cement is more abundant. Iron carbonate and sparry calcite cement rims quartz grains and is rimmed by kaolinite cement. Chlorite was found to rim both unaltered and kaolinized feldspars.

Iron-pore calcite occurs earliest and is followed by ferroan calcite in Frio sandstones in Brazoria County, whereas calcite leaching must have preceded or occurred contemporaneous with kaolinite cement (Kaiser and Richman, 1981). Previous work on the Frio 'A' sandstones at the Hitchcock N.E. field showed that iron-chlorite formation postdated quartz overgrowths and framboidal pyrite on which it has formed (Light, 1985). Only one horizontal muscovite flake showed kinking, and a deformation band extended from this kink into an adjacent quartz grain at 45 degrees to the direction of maximum stress.

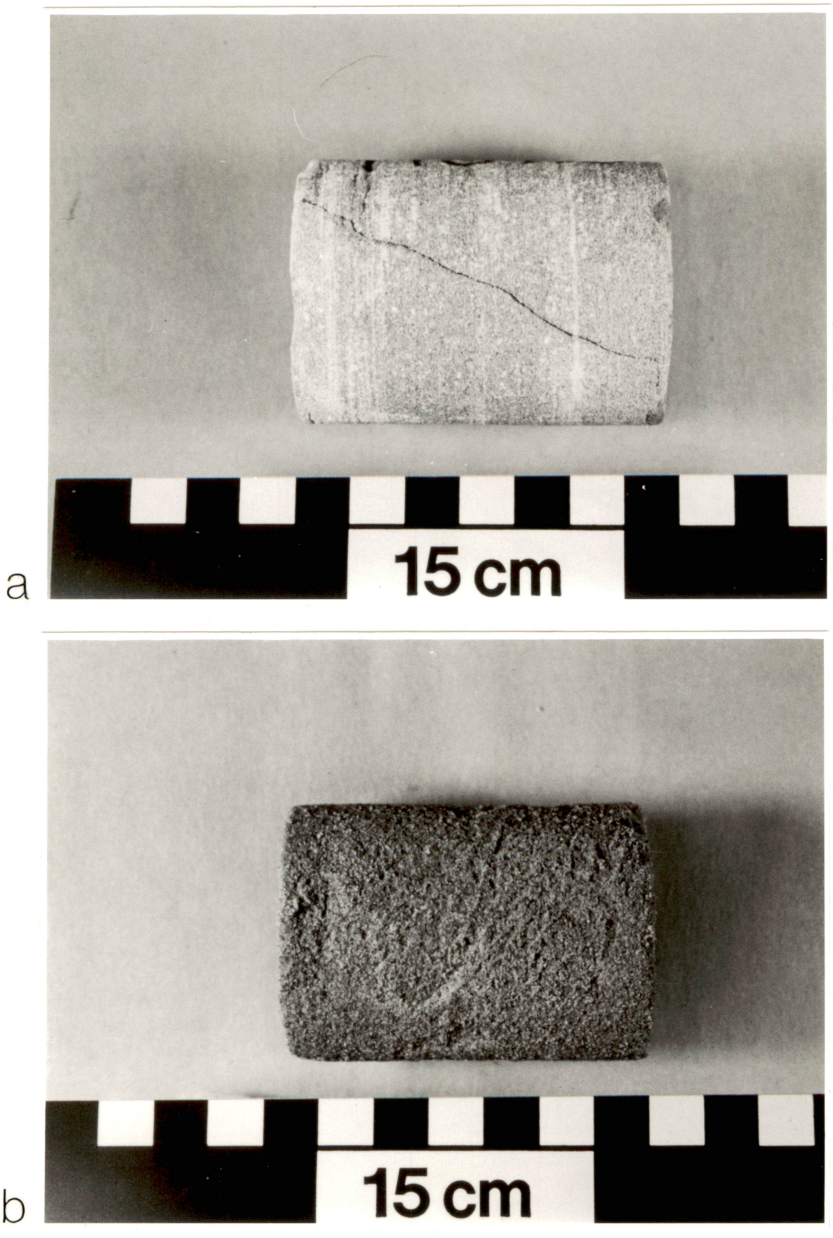


Figure 6. Experimentally compacted Frio 'A' sandstone cores showing (6a), excellent development of a crosscutting shear (9,189.5 ft, 2,801 m) and (6b) incipient development of a crosscutting shear (9,166 ft, 2,793 m).

## Diagenetic Textures of Distributary-Mouth-Bar Sandstones

The medium-grained distributary-mouth-bar sandstone at 9,166 ft (2,794 m) is very clean, well sorted, relatively uncemented, and friable. An incipient shear fracture has formed in the experimentally compacted core and dips at 55 degrees (fig. 6b). This shear fracture shows no visible extension and is rimmed by a zone some 3 to 5 mm wide where the rock has almost retained its original precompaction porosity.

In addition to the mineral assemblage already described, the mouth-bar sandstone also contains glauconite, perfectly rounded quartz grains, and extremely elongated feldspar laths, probably of eolian and volcanic origin, respectively. Feldspars were vacuolized during secondary porosity formation. Dolomite rhombohedrons are locally replaced by iron carbonate. However, carbonate forms a trace cement in this rock, whereas kaolinite is more abundant. Deformed shale clasts occur intergranularly to quartz and feldspar grains in the undeformed rock.

In the compacted sandstone at 9,166 ft (2,794 m)(fig. 6b), some deformation structures can be attributed to the experimentally imposed stress. One quartz grain showed strong deformation bands developed at 36 degrees to the maximum stress. Two quartz grains had an intergrown (stylolitized) contact, suggesting pressure solution effects. One horizontal elongated plagioclase lath was kinked and fractured over a quartz grain cut by a throughgoing shear at 45 degrees to the principal stress.

The experimentally compacted mouth-bar sandstone at 9,177.5 ft (2,797.3 m) shows the development of two sets of fractures (fig. 7a and 7b). A listric shear fracture has a dip that varies from 22 degrees at the top to 29 degrees at the base. Part of the shear is represented by a system of en echelon shears along which it has stepped laterally while it is crosscut by a second group of shorter incipient shears dipping at 45 degrees in the opposite direction. The major listric shear is refracted into bedding at the center of the core where a horizontal extension fracture has

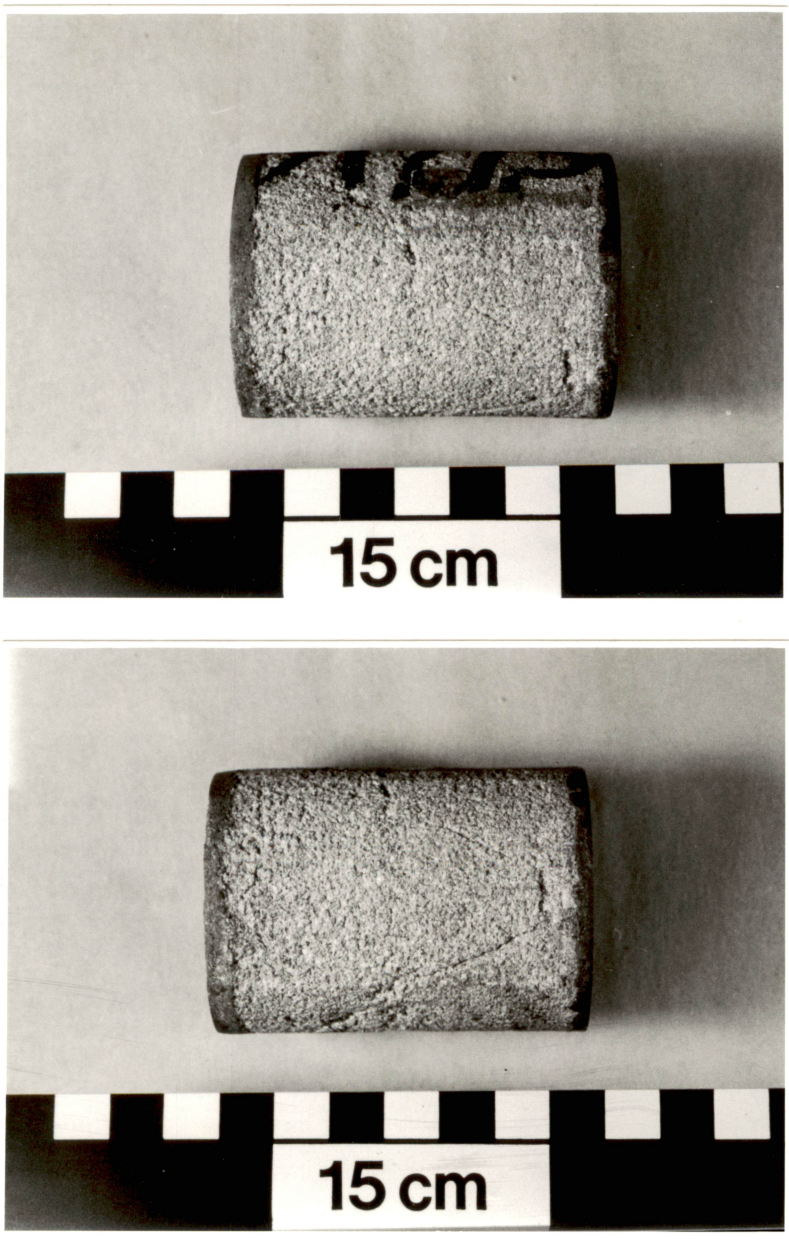


Figure 7. Experimentally compacted Frio 'A' sandstone core (9,177.5 ft, 2,797 m) showing development of intersecting horizontal and shear fracture sets.

formed on the downthrown side of the shear. The arrangement of an extension fracture on one side of the core which terminates against, but displaces a shear on the other side suggests that the core may not have been compressed uniformly during the compaction experiments. However, the very irregular, cavernous, and intergranular nature of the horizontal extension fracture suggests that it is a post-compaction expansion break.

The indurated distributary-mouth-bar sandstone at 9,177.5 ft (2,797.3 m) has a mineral assemblage similar to that of sandstones already described but contains in addition clear to milky quartz with quartz overgrowths, reddish microclines, kaolinized feldspars and carbonaceous fragments, glauconite, and a trace of amphibole. Kaolinite cement is fairly abundant and sporadically fills cavities between grains, giving a spotty appearance to the rock. Reddish-brown iron carbonate forms a trace cement but rims quartz overgrowths, indicating that it is a subsequent event.

Secondary dissolution porosity has formed from the partial or complete vacuolization of feldspar (particularly plagioclase), which has resulted in only the rims of some crystals remaining. Some feldspar overgrowths are formed of microcline, which surrounds an inner rim and corroded core of remnant iron carbonate. Kaolinite has cemented completely vacuolized feldspars in which only the feldspar overgrowth has remained intact. Evidently during the diagenesis some feldspars were overgrown with feldspar and subsequently the core was replaced by iron carbonate. Later these iron carbonates and feldspars were corroded and the rock cemented erratically by kaolinite.

One elongated quartz grain oriented perpendicular to the principal stress in the mouth bar sandstone at 9,177.5 ft (2,797.3 m) was kinked and had deformation bands oriented at 45 degrees to the major compression. One flake of muscovite mica oriented at 45 degrees to the principal stress had been kinked and crumpled and broken between adjacent quartz grains.

### Interpretation

The only clear evidence of intragranular deformation of grains within the Frio 'A' sandstones is the presence of deformation bands in some quartz and K feldspars oriented at 30 to 45 degrees to the principal stress, the kinking of horizontal or inclined elongated feldspars and micas, the crumpling and breaking of some inclined micas, and the collapse of vacuolized feldspars and remnant feldspar overgrowths. Vacuolized and skeletal feldspars represent about 2 percent of the volume of the sandstones, and complete collapse of these grains under experimental compaction would reduce the measured porosity by 7 to 10 percent of its original value. Shale and chlorite clasts have probably been further deformed and flattened, and there is some evidence of comminution of grains.

## POINT COUNT ANALYSES

Point count analyses were made of 18 vertical slides cut subperpendicular to bedding and parallel to core axes in both the uncompacted and experimentally compacted sandstones from the Delee No. 1 well (tables 1 and 2 and figs. 8, through 10). Two vertical sections (a-c and b-c axes, perpendicular to one another) were point counted for each core sample of both the uncompacted and the experimentally compacted material.

Minerals identified in the Frio 'A' sandstones were subjectively allocated to three main groups:

Brittle Grains

Quartz, feldspar, ore, igneous and metamorphic rock fragments, sandstone, siltstone, and chert

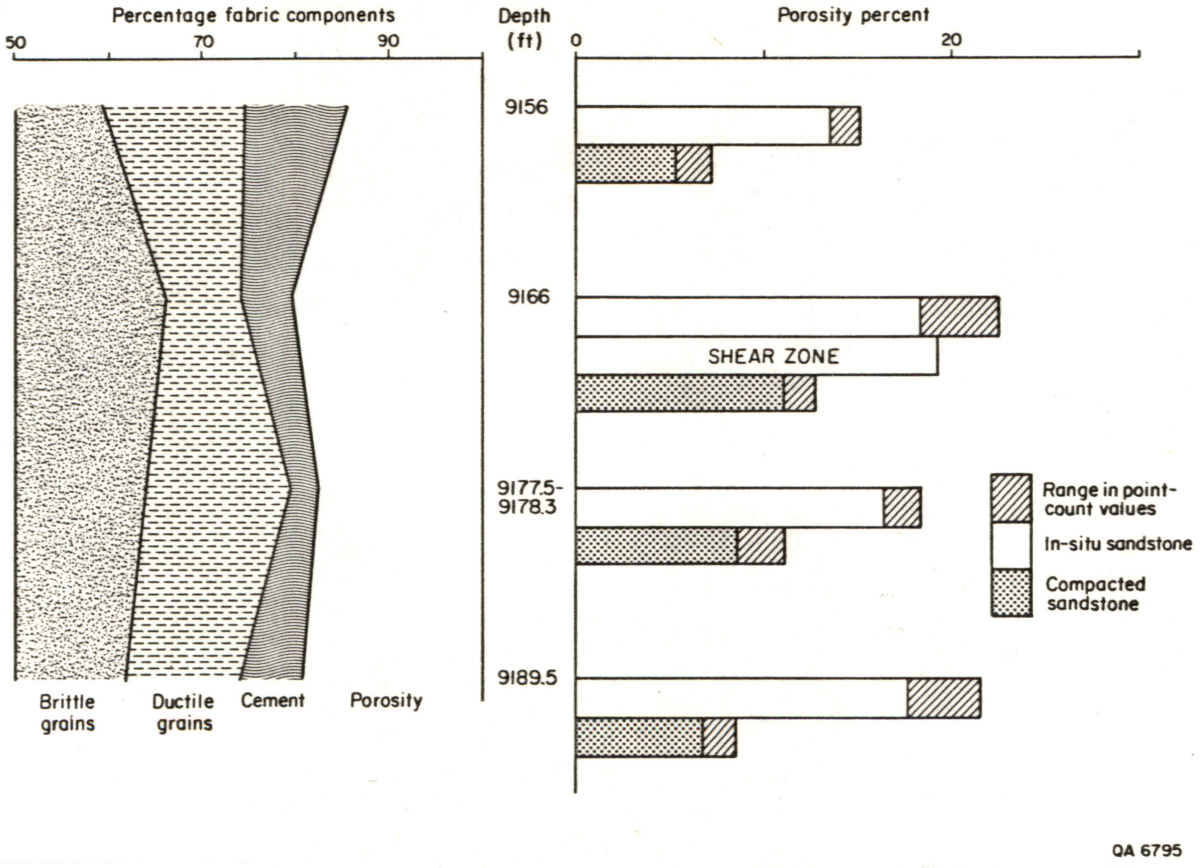


Figure 8. Porosity reduction in experimentally compacted Frio 'A' sandstones compared to the percentage content of fabric components.

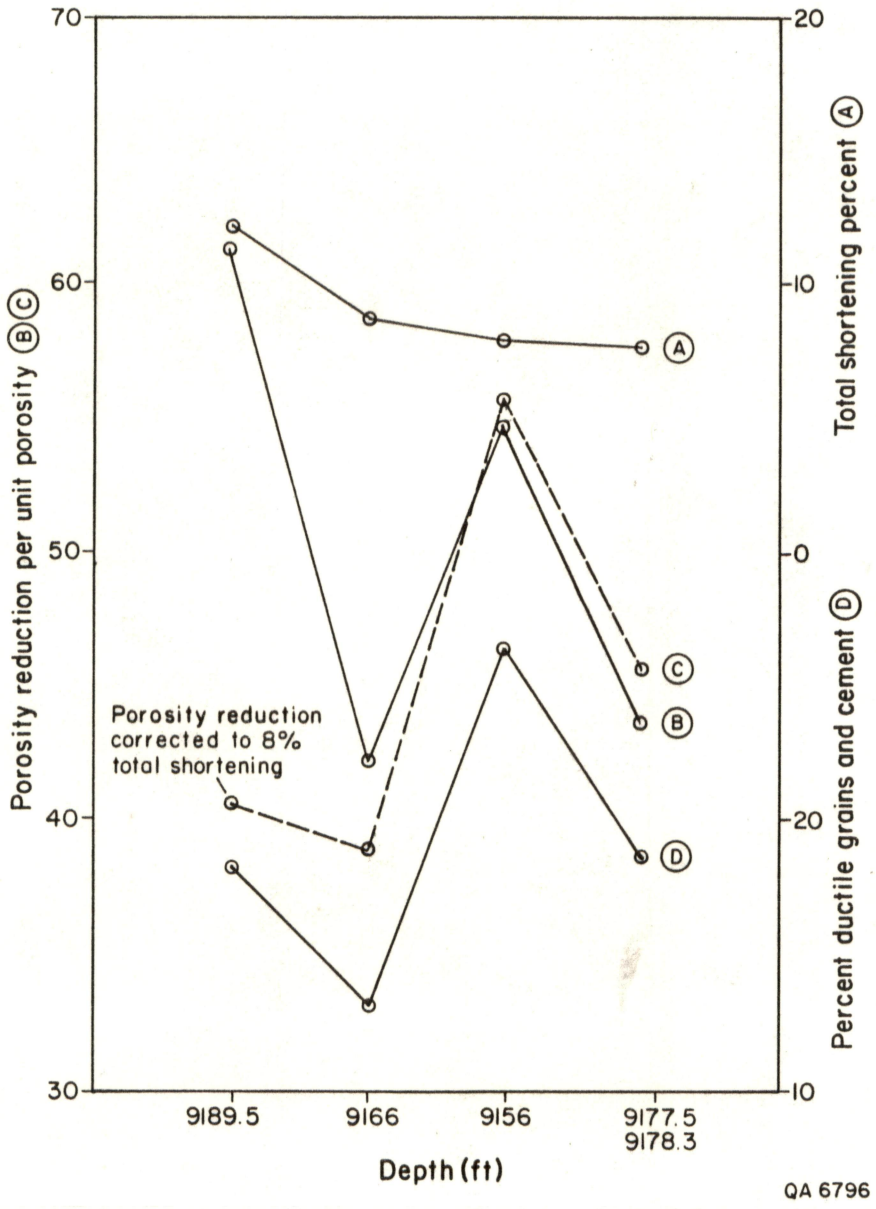


Figure 9. Total shortening in experimentally compacted Frio 'A' sandstones compared to the percentage content of ductile grains and cement and porosity reduction per unit porosity.

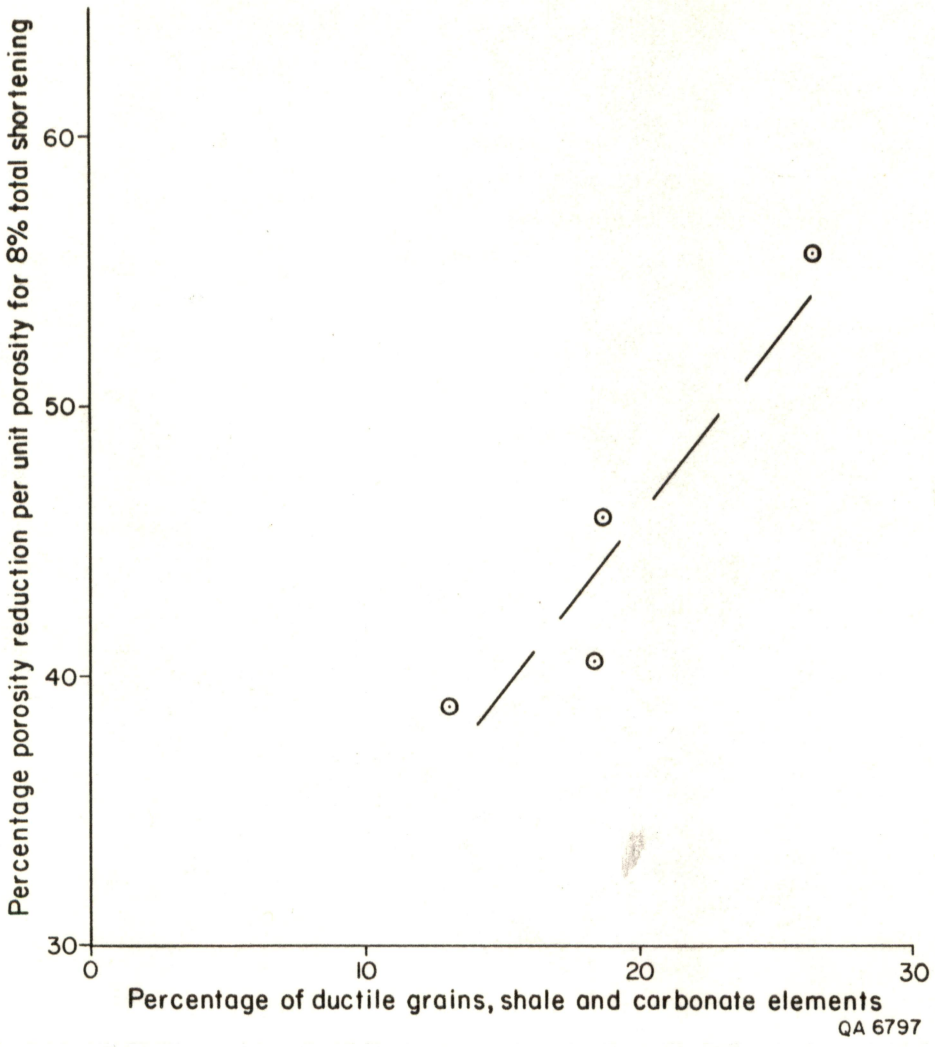


Figure 10. Percentage of ductile grains and carbonate cement in the Frio 'A' sandstones versus the percentage porosity reduction per unit porosity for 8 percent total shortening.

Ductile grains

Glauconite, chlorite, mica, chloritized volcanic rock fragments, and shale clasts

Cements

Sparry calcite, iron carbonate, kaolinite, and chlorite

Quartz and feldspar overgrowths have been included in the brittle grain group because they are generally well cemented onto sedimentary grains.

Total shortening (as measured by porosity reduction) for the Frio 'A' channel sandstones varies from 7.9 percent (9,156 ft, 2,791 m) to 12.1 percent (9,189.5 ft, 2,801 m)(table 2). The distributary-mouth-bar sandstones, however, show a more consistent total shortening of 7.6 percent (9,177.5 to 9,178.3 ft, 2,797.3 to 2,797.6 m) to 8.7 percent (9,166 ft, 2,794 m) consistent with them having a more highly winnowed, homogeneous nature. The process of shortening due to experimental compaction appears to have occurred almost entirely by grain rotation, intergranular (grain boundary) slip, and grain rearrangement with some grain comminution. There is a general lack of deformation fabrics that can be traced from one grain to the next.

The range in point count values for the porosity of the uncompacted and experimentally compacted sandstones is graphically displayed in figure 8 and compared to the abundance of fabric components. Porosity was also estimated within a 3 mm uncompacted zone adjacent to a shear in the friable mouth-bar sandstone at 9,166 ft (2,794 m) and is compared to the porosities away from the shear in uncompacted and compacted sandstones at the same depth (fig. 8). The relatively uncompacted shear zones developed along incipient shears in the experimentally compacted friable

mouth-bar sandstones at 9,166 ft (2,794 m) have retained almost their original pre-compaction porosities (table 1, fig. 8).

The greatest porosity reduction per unit porosity (61.3 percent) is shown by the channel sandstone at 9,189.5 ft (2,801 m), which contains 18.5 percent of ductile grains and cements (fig. 1, table 2). In contrast, in the channel sandstone at 9,156 ft (2,791 m) porosity reduction per unit porosity is 54.7 percent, and it contains 26.4 percent of ductile grains and cements (fig. 1, table 2). Evidently such large porosity reductions cannot result from collapse of skeletal or vacuolized feldspars because the latter could only produce a 7 to 10 percent porosity reduction per unit porosity.

The trend of the percent porosity reduction curve for the experimentally compacted Frio 'A' sandstones is similar to the trend of abundance of ductile grains and cements in the sandstones, particularly when normalized to 8 percent total shortening (fig. 9). At 8 percent total shortening there is an approximate linear relationship between the normalized percent porosity reduction and the concentration of ductile grains, shale, chlorite, and carbonate cements (fig. 10). Evidently these ductile grains and cements have deformed and lubricated grain margins and thus facilitated intergranular rotation and movement, allowing greater degrees of relative shortening to occur where they are abundant. This appears to be the major mechanism by which the Frio 'A' sandstones have deformed during experimental compaction.

## GRAIN ORIENTATIONS IN VERTICAL SECTIONS

The long axes of grains were measured in vertical sections in both the uncompacted and compacted sandstones at the four core sample positions in the Frio 'A' sandstone (9,156 ft, 2,791 m; 9,189.5 ft, 2,801 m; 9,166 ft, 2,794 m; 9,177.5-

9,178.3 ft; 2,797.3, 2,797.6). Grain long axes were then digitized and plotted using the ROSEDIA program. Moving-average diagrams of the boundary of the radial distribution for cumulative percentage of axial length were found to give the best definition of the grain orientations and are shown in figures 11 through 14.

Most grains in the uncompacted fine to medium grained, calcareous channel sandstone at 9,156 ft (2,791 m) are oriented within 30 degrees of bedding (parallel to crossbeds/reverse imbricated?), whereas another major group shows normal imbrication inclined upslope between 20 and 30 degrees (fig. 11).

In the experimentally compacted sandstone (9,156 ft; 2,791 m), the group of imbricated grains has rotated through some 10 to 15 degrees toward the bedding, a result of vertical shortening of the sample. However an additional group of grains has rotated into a shear direction at an angle of 30 degrees to the maximum vertical stress (fig. 11). These shear-oriented grains are probably derived from reorientation of steeply dipping normal and reverse imbricated grains (fig. 11). Reorientation of grains into a shear direction would allow them to move through the bedding surfaces to fill vacant pore spaces and produce a closer packed fabric.

The uncompacted, highly indurated channel sandstone at 9,189.5 ft (2,801 m) contains a major proportion of grains normally imbricated at angles of 15 to 75 degrees to bedding, whereas a smaller group lies subparallel to bedding (fig. 12). Some grains have axial orientations between those of the imbricated and normally bedded particles (fig. 12).

Experimental compaction of the channel sandstone at 9,189.5 ft (2,801 m) has resulted in major reorientation of imbricated grains parallel to bedding through at least 35 degrees. In addition some grains in the compacted sandstone have become reoriented vertically, parallel to probable extension fractures and at 30 degrees from vertical parallel to incipient shear trends (fig. 12). The presence of a large percentage

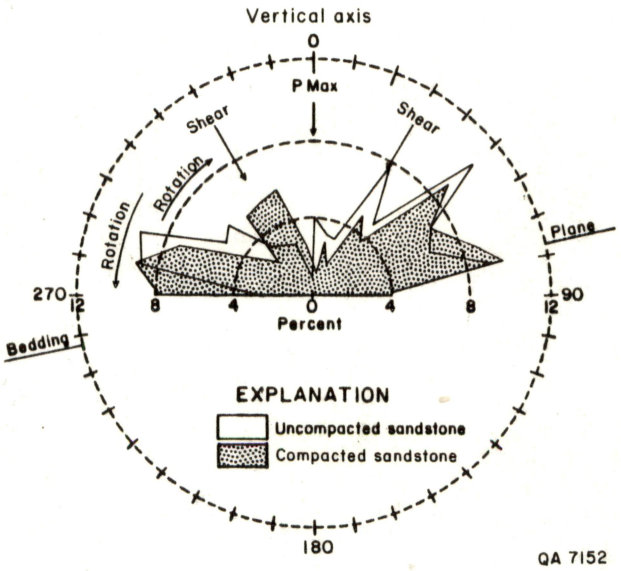


Figure 11. Comparative rose diagram showing the cumulative percent orientation of grain long axes for uncompacted and experimentally compacted Frio 'A' sandstones (9,156 ft, 2,791 m).

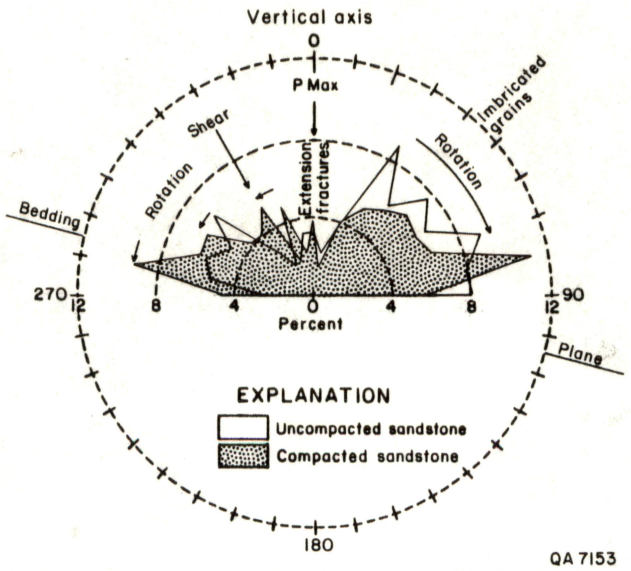


Figure 12. Comparative rose diagram showing the cumulative percent orientation of grain long axes for uncompacted and experimentally compacted Frio 'A' sandstones (9,189.5 ft, 2,801 m).

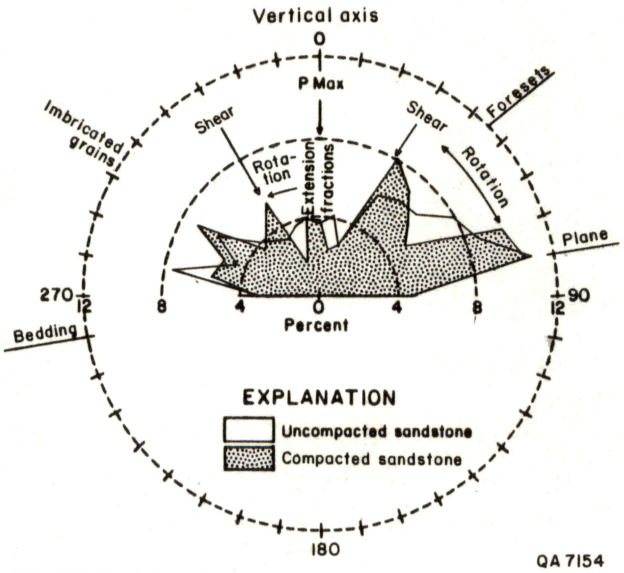


Figure 13. Comparative rose diagram showing the cumulative percent orientation of grain long axes for uncompacted and experimentally compacted Frio 'A' sandstones (9,166 ft, 2,794 m).

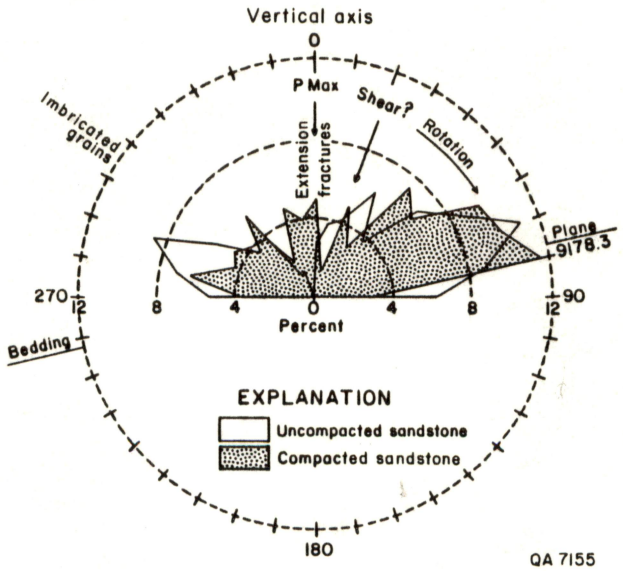


Figure 14. Comparative rose diagram showing the cumulative percent orientation of grain long axes for uncompacted (9,178.3 ft, 2,797.6 m) and experimentally compacted (9,177.5 ft, 2,797.3 m) Frio 'A' sandstones.

of imbricated grains at steep angles to bedding and intergranular ductile materials (18.5 percent, table 3) in the uncompacted sandstone has facilitated the movement of grains through bedding into vacant pore spaces during compaction. Grain movement has resulted in the large total shortening shown by the sample (12.1 percent, table 2) and the well-developed, close packed fabric (fig. 16d, table 4). Across-bed movement may have been assisted by reorientation of some grains to shear and extension fracture trends.

The friable distributary-mouth-bar sandstone at 9,166 ft (2,794 m) contains the smallest percentage of intergranular ductile and carbonate material (table 2) and shows the least measured total shortening (7.9 percent, table 2). Most grains in the uncompacted mouth-bar sandstone at 9,166 ft (2,794 m) are normally imbricated at an angle of about 30 to 35 degrees with respect to foresets (dipping at 45 degrees to left, fig. 13). A smaller percentage of grains is normally imbricated at angles of 22 to 35 degrees with respect to the bedding while a smaller concentration is perpendicular to bedding (fig. 13).

Experimental compaction of the mouth-bar sandstone at 9,166 ft (2,794 m) has resulted in the major rotation of grains, imbricated at less than 30 degrees with respect to foresets, by more than 35 degrees into a shear orientation at 30 degrees from the vertical maximum stress (fig. 13). Grains that are imbricated at angles steeper than 30 degrees to the foresets have been rotated toward bedding. A similar rotation of grains oriented perpendicular to bedding into shear and extension fractures has also occurred (fig. 13). The final distribution of a large group of grain axes along shear trends at 30 degrees from the principal stress also results in these grains being oriented subparallel and almost perpendicular to the original foreset beds (fig. 13). Evidently the principal mechanism of compaction in this friable rock was by movement

Table 3. Comparison of fabrics of uncompacted and compacted sandstones for vertical sections almost perpendicular to bedding.

| | Distributary Channel Sandstones | | Distributary Mouth Bar Sandstones | |
|---|---|---|---|---|
| | 9,156.06 ft | 9,189.5 ft | 9,166.0 ft | 9,177.5 ft<br>9,178.3 ft |
| **Induration** | Moderately indurated | Highly indurated | Friable | Highly indurated |
| **Percent Ductile Grains and Carbonate Cement** | 26.4 | 18.5 | 13.1 | 18.7 |
| **Total Shortening** | 7.9 | 12.1 | 8.7 | 7.6 |
| **Primary Textures** | Normal and reverse?-imbricated crossbeds | Normal and reverse?-imbricated bedding | Normal and reverse?-imbricated cross beds | Normal and reverse?-imbricated cross beds |
| **Bedding Inclination** | 13° dip to 270° | 15° dip to 90° | 10° dip to 270° | 13° dip to 270° |
| **Initial Strain Ellipse** | Well developed parallel to bedding<br>RI=1.6 | Well developed parallel to imbrication<br>RI=1.9 | Well developed parallel to imbrication and bedding<br>RI=1.1 | Well developed parallel to imbrication and bedding<br>RI=1.9 |
| **Compaction Strain Ellipse** | Poorly developed parallel to shear direction<br>RI=1.3 | Well developed horizontal bedding<br>RI=2.1 | Well developed parallel to imbrication<br>RI=1.3 | Well developed parallel to imbrication<br>RI=1.5 |
| **Percentage Change in Axial Ratio** | Decreased by 17.4% (oblate spheroid) | Increased by 13% | Increased by 14% | Decreased by 21% |
| **Initial Interference Patterns** | Weakly developed rhombic | Well developed rhombic | Well developed linear pattern parallel to foresets | Weakly developed rhombic |
| **Compaction Interference Patterns** | Well developed square | Well developed square | Not discernable | Well developed rhombic |
| **Interpretation of Grain Movement** | Steeply dipping normal imbricated grains rotated into shear direction. Shallowly dipping normal imbricate grains rotated into bedding pore spaces to produce a well developed close packed fabric | Reverse imbricated grains rotated into shear and extension fracture trend. Normal imbricated grains rotated into bedding pore spaces to produce a well developed close packed fabric | Normal imbricated cross bed oriented grains rotated into shear and extension fracture trends. Grains move into pore spaces to produce a poorly developed close packed fabric | Normal imbricated grains rotated into extension fracture trend. Grains move into pore spaces to produce a well developed close packed fabric |

Table 4. Comparison of fabrics of uncompacted and compacted sandstones for sections subparallel to bedding.

| | Distributary Channel Sandstones | | Distributary-Mouth-Bar Sandstones | |
|---|---|---|---|---|
| | 9,156.06 ft | 9,189.5 ft | 9,166.0 ft | 9,177.5 ft<br>9,178.3 ft |
| Induration | Moderately Indurated | Highly Indurated | Friable | Highly Indurated |
| Percent Ductile Grains and Carbonate Cement | 26.4 | 18.5 | 13.1 | 18.7 |
| Total Shortening | 7.9 | 12.1 | 8.7 | 7.6 |
| Initial Strain Ellipse | Poorly Developed Ellipse RI = 1.3 | Well Developed Ellipse RI = 1.6 | Poorly Developed Ellipse RI = 1.9 | Poorly Developed Ellipse RI = 1.5 |
| Compaction Strain Ellipse | Well Developed Ellipse RI = 1.6 | Poorly Developed Ellipse RI = 1.8 | Poorly Developed Ellipse RI = 2.4 | Poorly Developed Ellipse RI = 2.8 |
| Percentage Change in Axial Ratio | Increased by 20% | Increased by 10.4% | Increased by 27% | Increased by 77% |
| Initial Interference Pattern | Not Discernable | Well Developed Rhombic | Weakly Developed Rhombic | Weakly Developed Rhombic |
| Compaction Interference Pattern | Not Discernable | Well Developed Square | Weakly Developed Square | Weakly Developed Square |
| Comparison of percentage change in axial ratios of strain ellipses in sections parallel and perpendicular to bedding | | | | |
| Vertical Section | 17.4 | 13 | 14 | 21 |
| Horizontal Section | 20 | 10.4 | 27 | 77 |

of grains oriented parallel to shear and extension fracture trends, across and along foreset bedding into empty pore spaces to produce a weakly developed, close packed fabric.

The very indurated distributary-mouth-bar sandstones at 9,178.3 ft (2,797.6 m) (uncompacted) and 9,177.5 ft (2,797.3 m) (experimentally compacted) are not as comparable as samples discussed earlier because they come from slightly different depths. However, in the composite rose diagram (fig. 14) most of the long axes of grains are found to be oriented within 20 degrees of the bedding, whereas an additional group are normally imbricated at 10 and 50 degrees to the bedding trend. In the experimentally compacted sandstone at 9,177.5 ft (2,797.3 m) a large group of imbricated grains has rotated into an extension fracture orientation (fig. 14), which probably represents the direction along which grains moved across bedding into vacant pore spaces during compaction.

## INTERFERENCE PATTERNS

The initial and experimentally compacted fabrics of the sandstones from the Delee No. 1 well were found to produce different interference patterns in the Fry (1979) diagrams, both in the region directly around the central vacancy field (Ramsay and Huber, 1983) and across the whole area. In order to elucidate these interference patterns Fry (1979) patterns were constructed for several artificial grain center arrangements with different packing fabrics (fig. 15). Ellipses with different axial ratios were used in these diagrams as there is a marked degree of elongation shown by quartz and feldspar grains in the uncompacted sandstones.

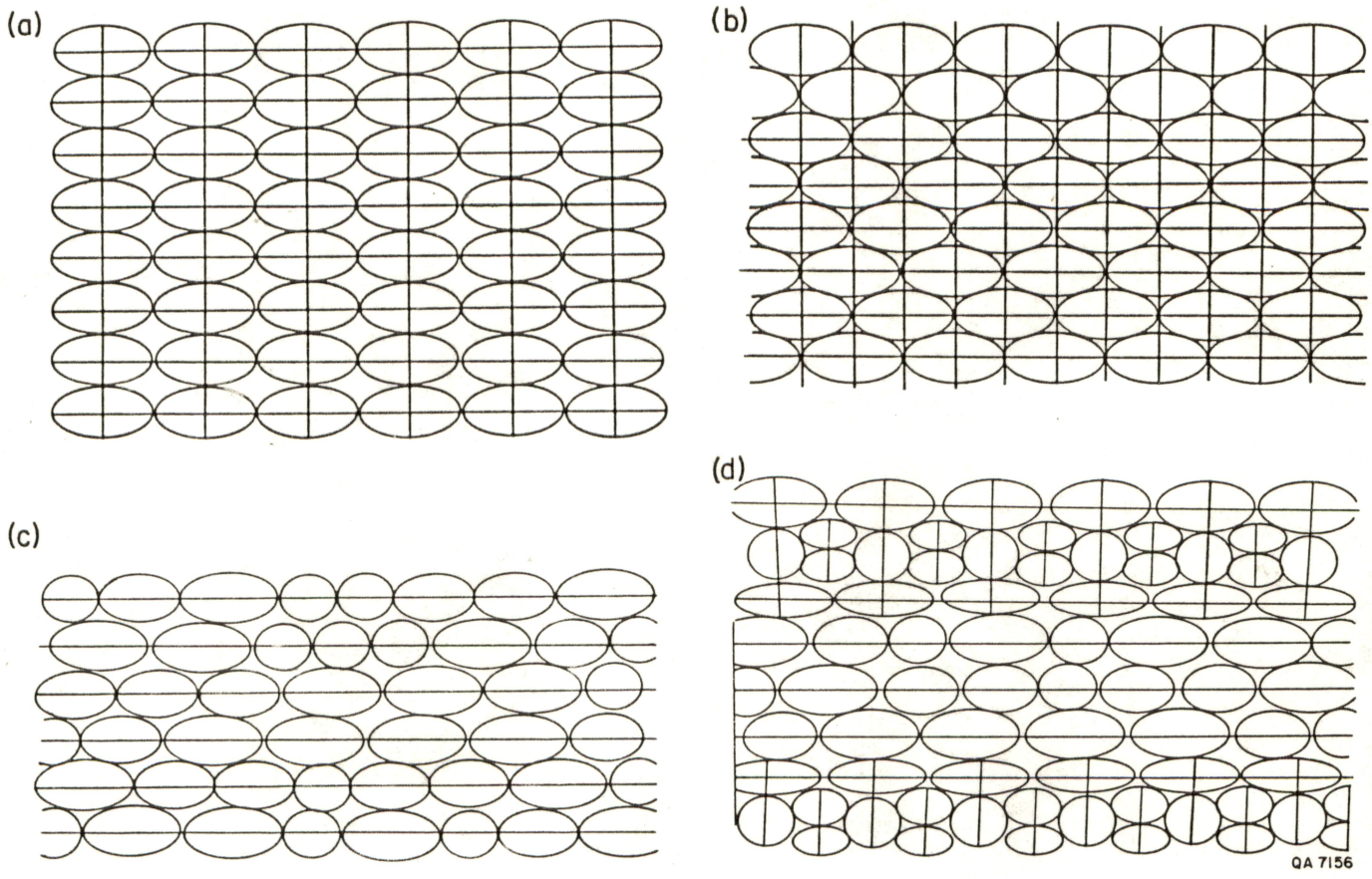


Figure 15. Open packed (15a) and closely packed (15b) ellipses. Randomly positioned ellipse centers (15c) in a uniformly thick bedding. 15d. Combination of randomly spaced centers along uniformly thick bedding and a closely packed structure of varying ellipse size. Fry (1979) diagrams constructed from these figures were used to interpret the Frio 'A' sandstone fabrics.

Open-packed ellipses (fig. 15a) produce a rhombic vacancy field (fig. 16a), which is most clearly demonstrated by the vacancy field of the uncompacted Frio 'A' sandstone at 9,189.5 ft (2,800 m)(figs. 16c and 16e). Closely packed ellipses (fig. 15b) produce a squarer vacancy field (fig. 16b) distinctly visible in the vacancy field for the experimentally compacted Frio 'A' sandstone at 9,189.5 ft (2,800 m)(figs. 16d and 16f). Evidently the experimental compaction has resulted in the rearrangement of the grains in the sandstone (9,189.5 ft, 2,800 m) such that the packing has changed from a more open packed to a tighter, closely packed structure. The compaction induced grain movement and consequent packing rearrangement have visibly reduced the porosity in the sandstone at 9,189.5 ft (2,800 m) when the uncompacted (fig. 16e) and experimentally compacted sandstones (fig. 16f) are compared.

Interference patterns can be developed synthetically in the region around the central vacancy field of a Fry (1979) plot by randomly spacing grain centers (ellipses of different axial ratio with the same minor axis) along uniformly thick bedding planes (fig. 15c). In this case a strong interference banding is developed parallel to the bedding and spaced at the bedding thickness (fig. 17a). Similarly a patchwork "cross hatched" interference pattern (fig. 17b) results from the combination of uniformly thick beds having randomly spaced grain centers and sets of intermediate beds having a close packed structure (fig. 15d). In this complex interference pattern, the horizontal interference banding records individual bedding planes while thicker interference zones mimic the stacked sets of beds that have differing packing arrangements.

The uncompacted (very friable) sandstone at 9,166.0 ft (2,794 m) has a well-defined interference banding in the Fry (1979) diagram, which appears to result from the preferential arrangement of grain centers along lines at a steep angle to the sedimentation unit boundaries (fig. 17c and 17d). However the strain ellipsoid is

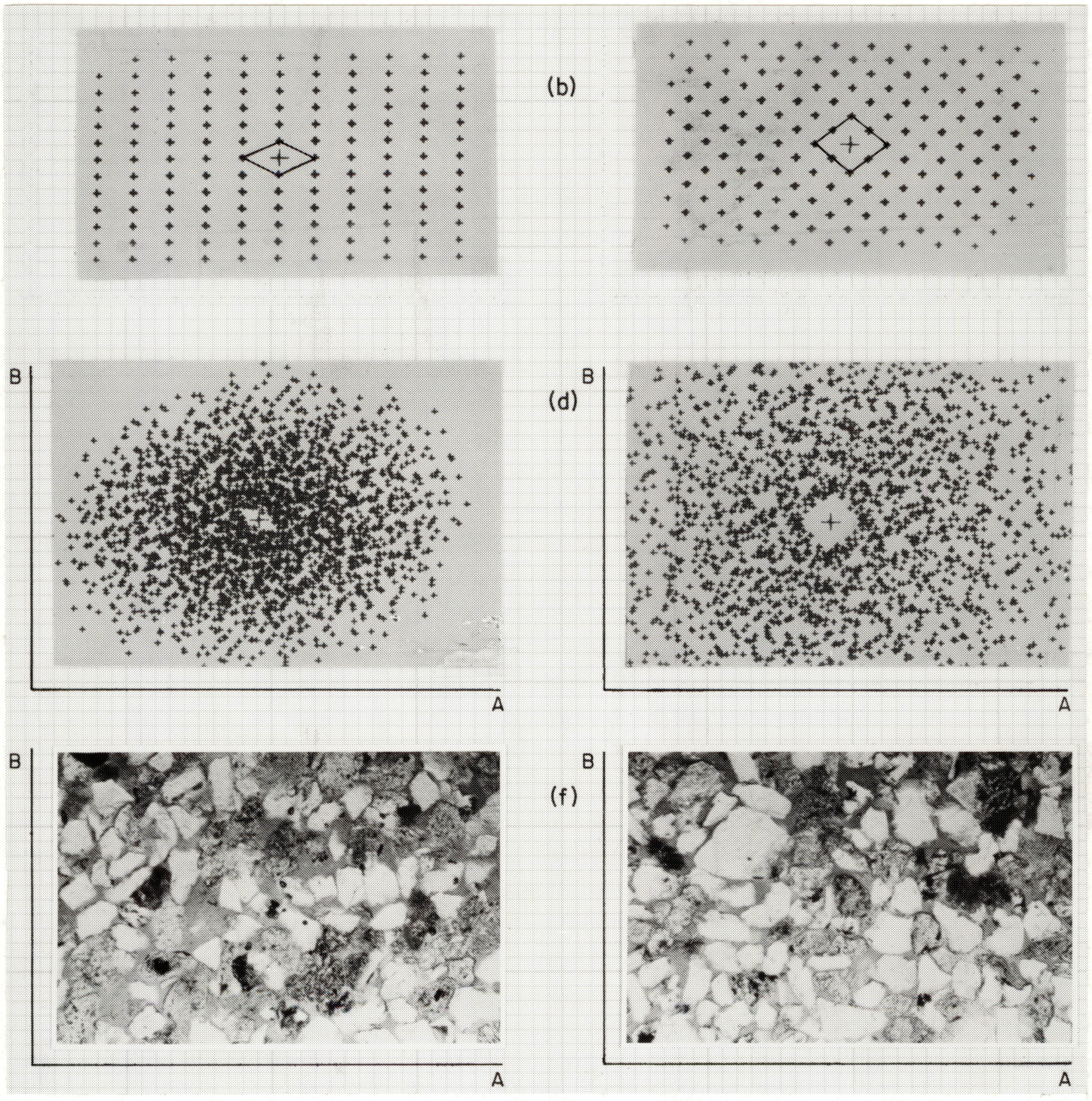


Figure 16. Fry (1979) diagrams for open packed (16a) and more closely packed (16b) ellipses compared to the uncompacted (16c, 16e) and compacted (16d, 16f) Fry (1979) diagrams for Frio 'A' sandstones (9,189.5 ft, 2,800 m). Porosity reduction is clearly seen when the the uncompacted sandstone (16e) is compared to the compacted sandstone (16f).

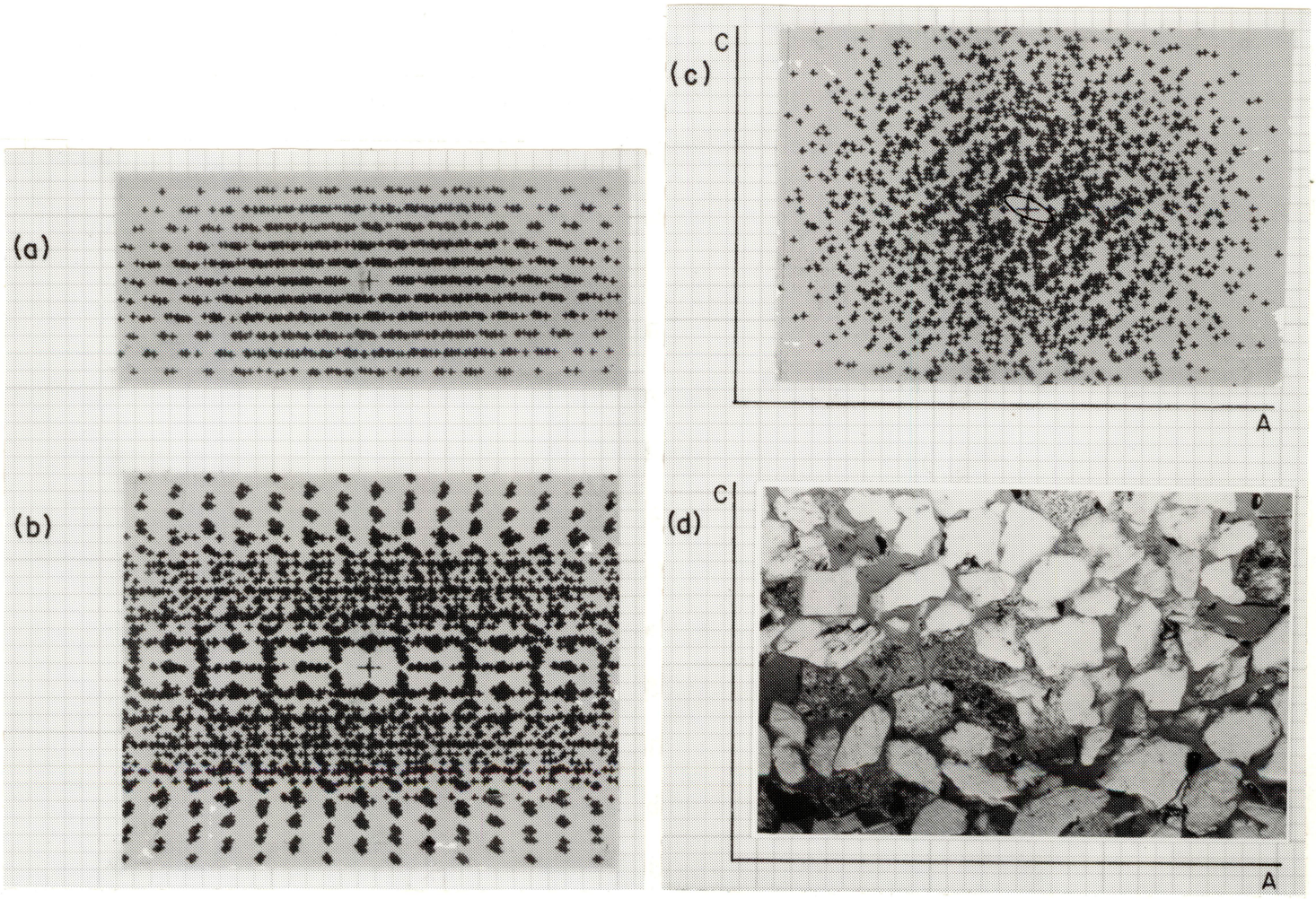


Figure 17. Fry (1979) diagram (17a) showing a well developed interference banding due to random spacing of ellipse centers along uniformly thick beds (see 15c). Fry (1979) diagram (17b) showing a well developed "cross hatched" interference pattern which mimics layering of the ellipse fabric (15d) used to construct it. Fry (1979) diagram (17c) for a vertical plane in an uncompacted Frio 'A' sandstone (9,166 ft, 2,794 m) showing a steeply dipping interference banding. Plate (17d) showing preferential arrangement of grain centers along steeply dipping foreset beds (?) oblique to bedding in the uncompacted sandstone (9,166 ft, 2,794 m).

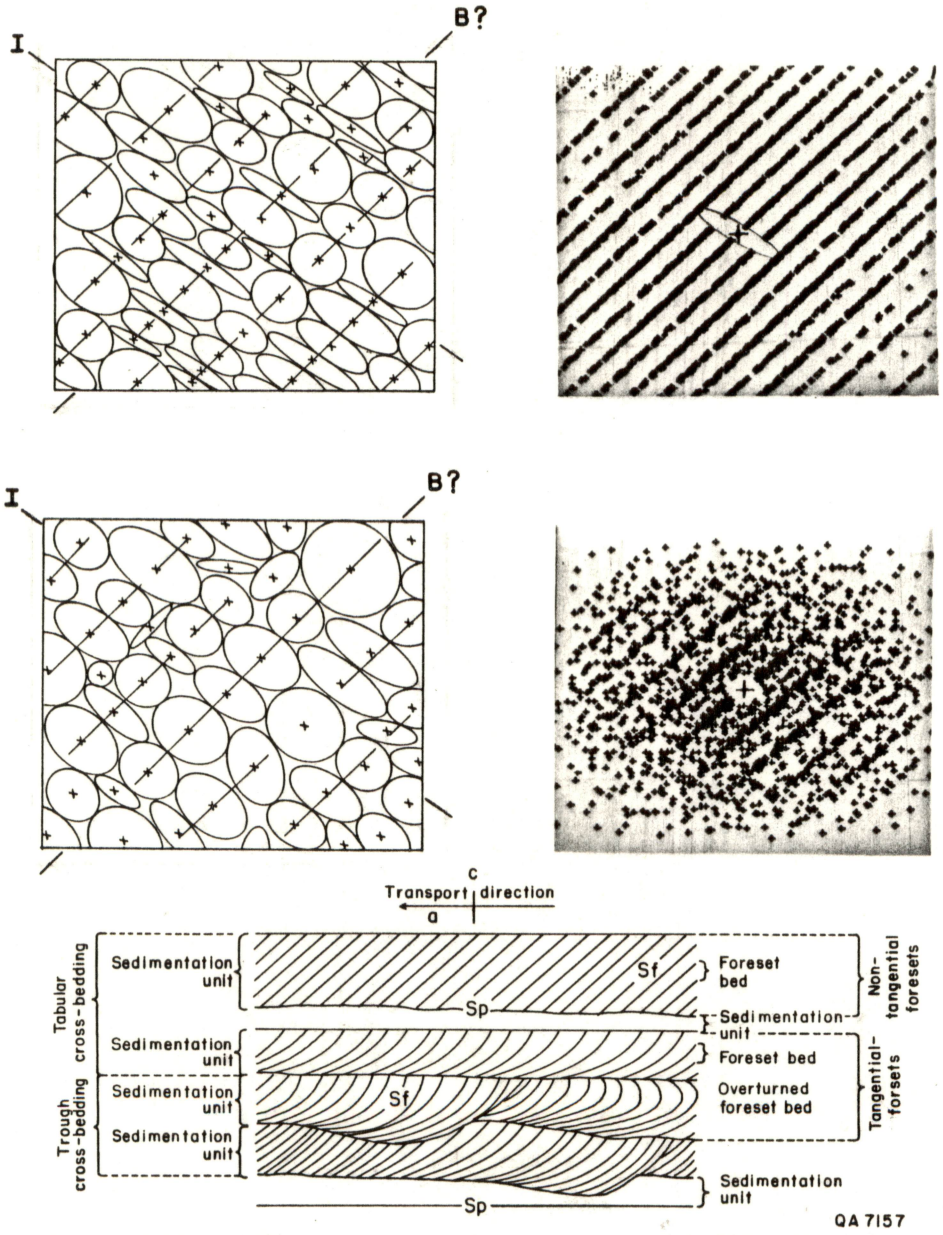


Figure 18. Fry (1979) diagrams for highly elongated ellipses stacked in imbricated foreset beds (18a and 18b) and more rounded ellipses stacked in imbricated foreset beds (18c and 18d). Steeply dipping interference banding in 18d closely mimics the pattern seen in 17c. However average elongation of grains in 17d lies between that of 18b and 18d. The relationship of foreset beds to transport direction and sedimentation unit boundaries is shown in 18e (after Potter and Pettijohn, 1977).

Comparison of Fry (1979) diagrams of vertical sections through the uncompacted (fig. 17c) and compacted sandstones (fig. 20a) at 9,166 ft (2,794 m), though clearly showing a loss of the linear (foreset) interference banding with compaction due to grain movement, does not define the precise nature of the packing.

Weak interference patterns are discernible on horizontal Fry (1979) diagrams for both the uncompacted (rhombus) and the experimentally compacted sandstones (square) at 9,166 ft (2,794 m)(table 4), which suggests a tightening of packing in the bedding from more open packed to a more closely packed structure.

Fry (1979) diagrams for vertical sections through the uncompacted sandstones at 9,156 ft (2,791 m), 9,178.3 ft (2,797.6 m), and 9,189.5 ft (2,801 m) (figs. 19a, 19b, and 19c) show diffuse rhombic interference patterns that result from the open packed nature of the sediments. The Fry (1979) diagrams for vertical sections through experimentally compacted sandstones at 9,156 ft (2,791 m) and 9,189.5 ft (2,801 m) (figs. 20b and 20d) show square interference patterns that result from a more closely packed fabric. Fry (1979) diagrams for vertical sections through experimentally compacted (9,177.5 ft, 2,797.3 m) uncompacted sandstones (9,178.3 ft, 2797.6 m) (figs. 19b and 20c) show similar rhombic interference patterns, suggesting that little change in packing has occurred in the vertical plane.

In horizontal sections, as already mentioned, Fry (1979) diagrams for uncompacted sandstones at 9,189.5 ft (2,801 m) show well-developed rhombic interference patterns, whereas in the experimentally compacted sandstones the pattern is square, indicating a change in packing from open to close (figs. 16c and 16d, table 4). Similar but more poorly defined change in packing from rhombic (open packing) to square (close

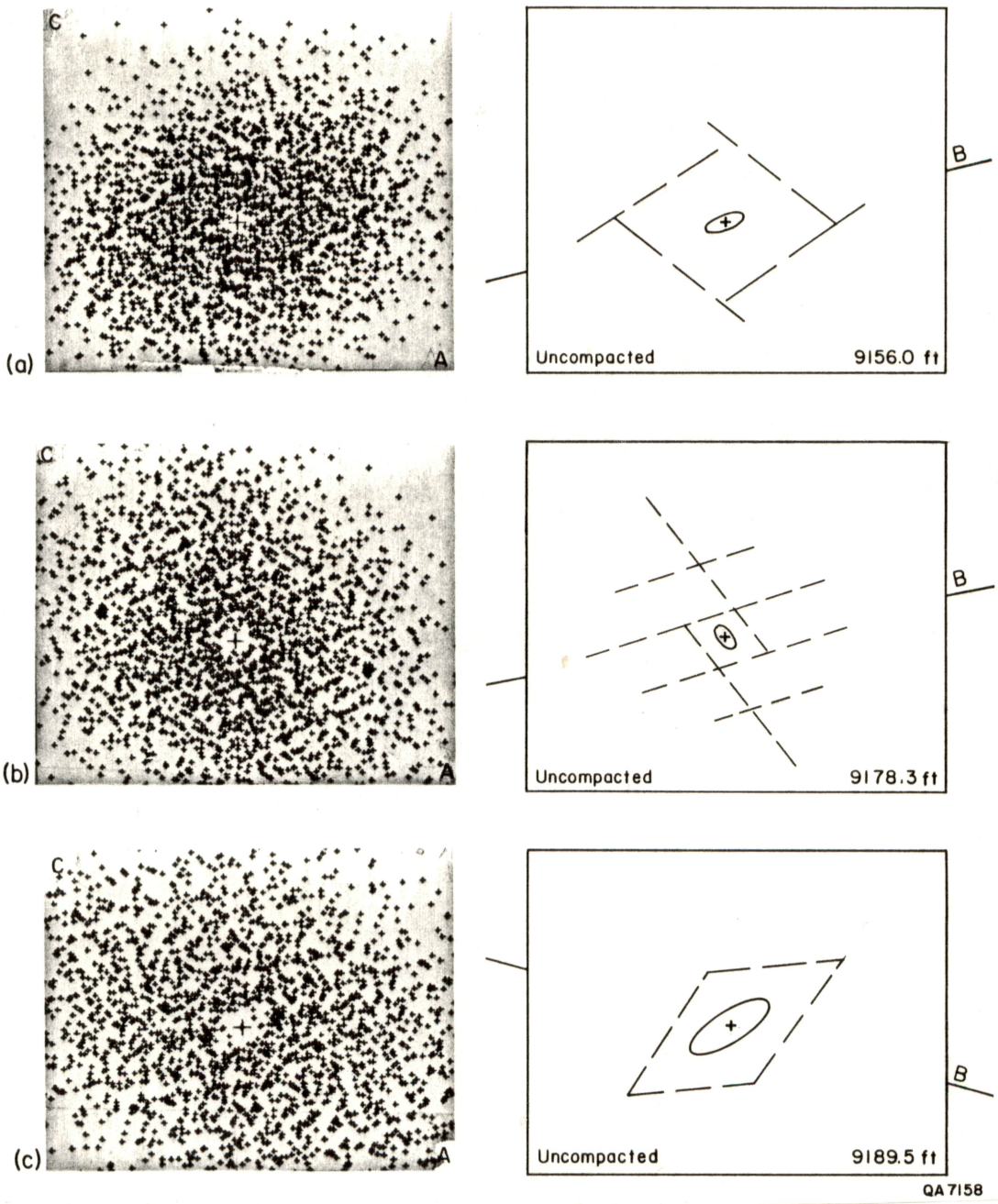


Figure 19. Fry (1979) diagrams for vertical planes in uncompacted sandstones at 9,156 ft (2,791 m) (19a), 9,178.3 ft (2,797.6 m) (19b), and 9,189.5 ft (2,801 m). Poorly developed rhombic interference patterns suggest that these rocks are generally open packed.

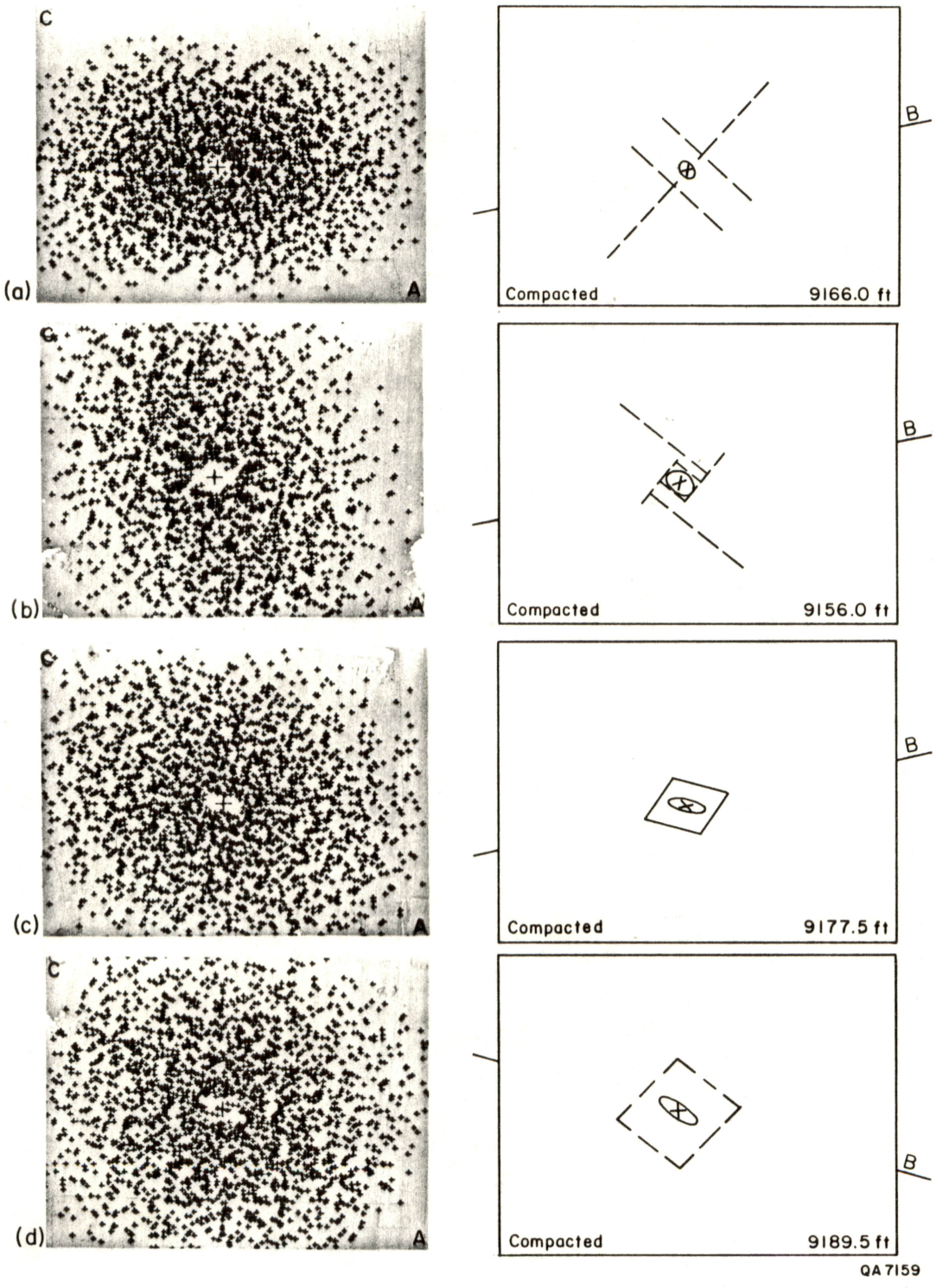


Figure 20. Fry (1979) diagrams for vertical planes in experimentally compacted sandstones at 9,166 ft (2,794 m)(20a), 9,156 ft (2,791 m)(20b), 9,177.5 ft (2,797.3 m) (20c), and 9,189.5 ft (2,801 m). Poorly developed cubic interference patterns suggest that the sandstones at 9,166 ft (2,794 m), 9,156 ft (2,791 m), and 9,189.5 ft (2,801 m) are more closely packed. The compacted sandstone at 9,177.5 ft (2,797.3 m) has a rhombic interference pattern similar to its uncompacted equivalent (19b), suggesting that there has been little change in packing from compaction in a vertical plane in this rock.

packing) is visible in horizontal sections in the uncompacted (9,178.3 ft; 2,797.6 m) and experimentally compacted (9,177.5 ft, 2,797.3 m) sandstones (table 4).

Although interference patterns are discernible on vertical Fry (1979) diagrams (figs. 19a and 20b), they cannot be seen in horizontal sections for both the uncompacted and experimentally compacted sandstones at 9,156 ft (2,791 m)(table 4), which suggests that most of the grain movement has occurred in a vertical plane.

## INITIAL AND COMPACTION STRAIN ELLIPSOIDS

Strain ellipses were drawn within the vacancy fields on Fry (1979) diagrams for vertical and horizontal sections in both uncompacted and compacted sandstones (figs. 21, through 24, and tables 3 and 4).

A well-developed initial strain ellipse parallel to bedding is present in the vertical Fry (1979) diagram (50 grain centers) for the crossbedded channel sandstones at 9,156 ft (2,791 m) and has an axial ratio of 3. A more poorly developed strain ellipse with an axial ratio of 1.6 in the Fry (1979) diagram constructed from 204 grain centers is oriented parallel to crossbeds or reverse imbrication (fig. 21a, table 3).

Poorly developed strain ellipses are present in Fry (1979) diagrams (50 and 206 grain centers) in experimentally compacted sandstones at 9,156 ft (2,791 m) and have axial ratios that have been reduced to 1.3 (17.4 percent) (fig. 21b, table 3) for a vertical section and increased to 1.6 (20 percent) (fig. 21d, table 4) for sections subparallel to bedding. The strain ellipse remains oriented parallel to cross bedding in the compacted section (fig. 21b). Grains were rotated into bedding to reduce the

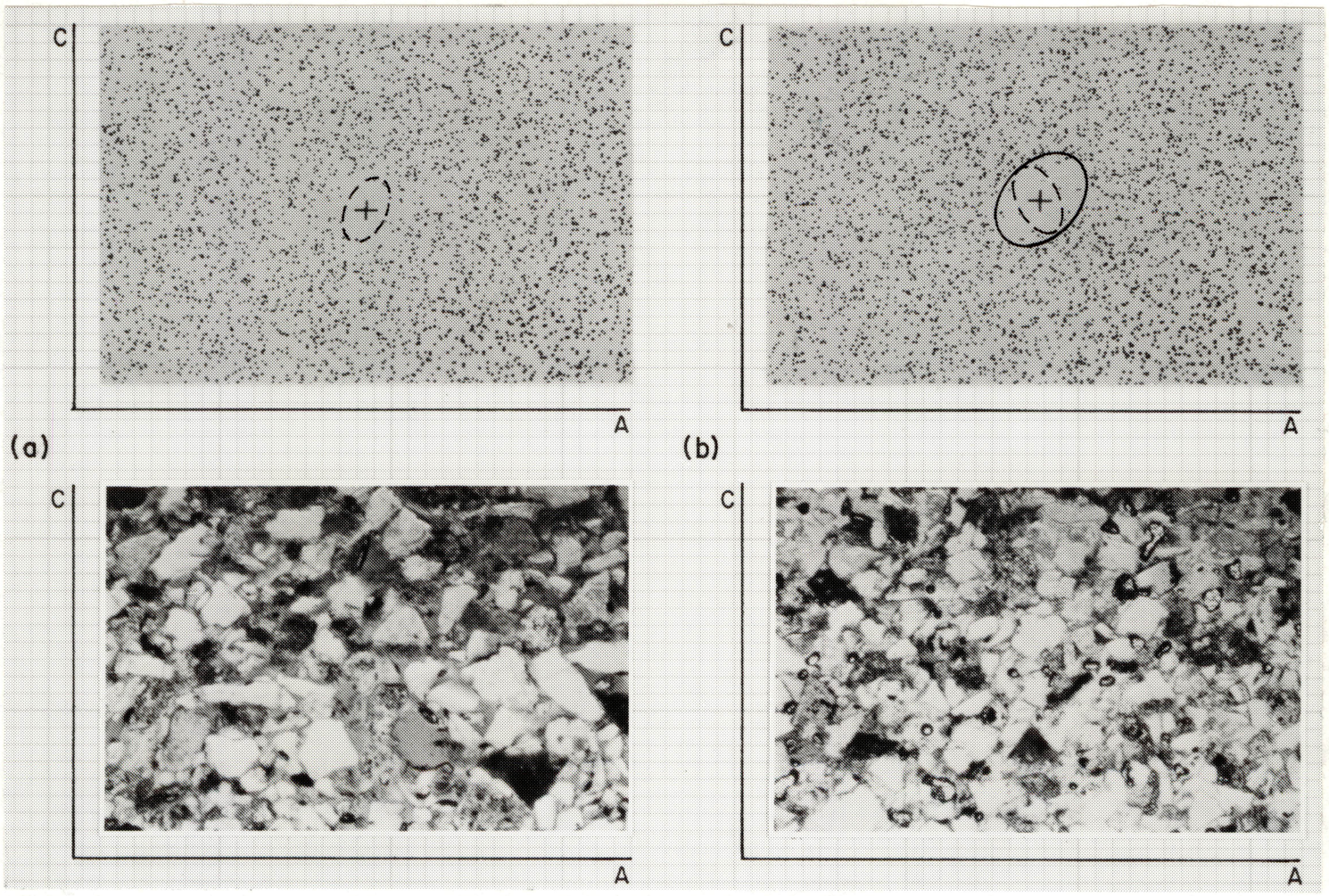


Figure 21. Fry (1979) diagrams for uncompacted (21a and 21c) and experimentally compacted (21b and 21d) Frio 'A' sandstones at 9,156 ft (2,791 m) with underlying plates showing grain fabric. The initial strain ellipse is elongated parallel to bedding in vertical sections (21a) where the greatest reduction in ellipse elongation from experimental compaction is evident (21b).

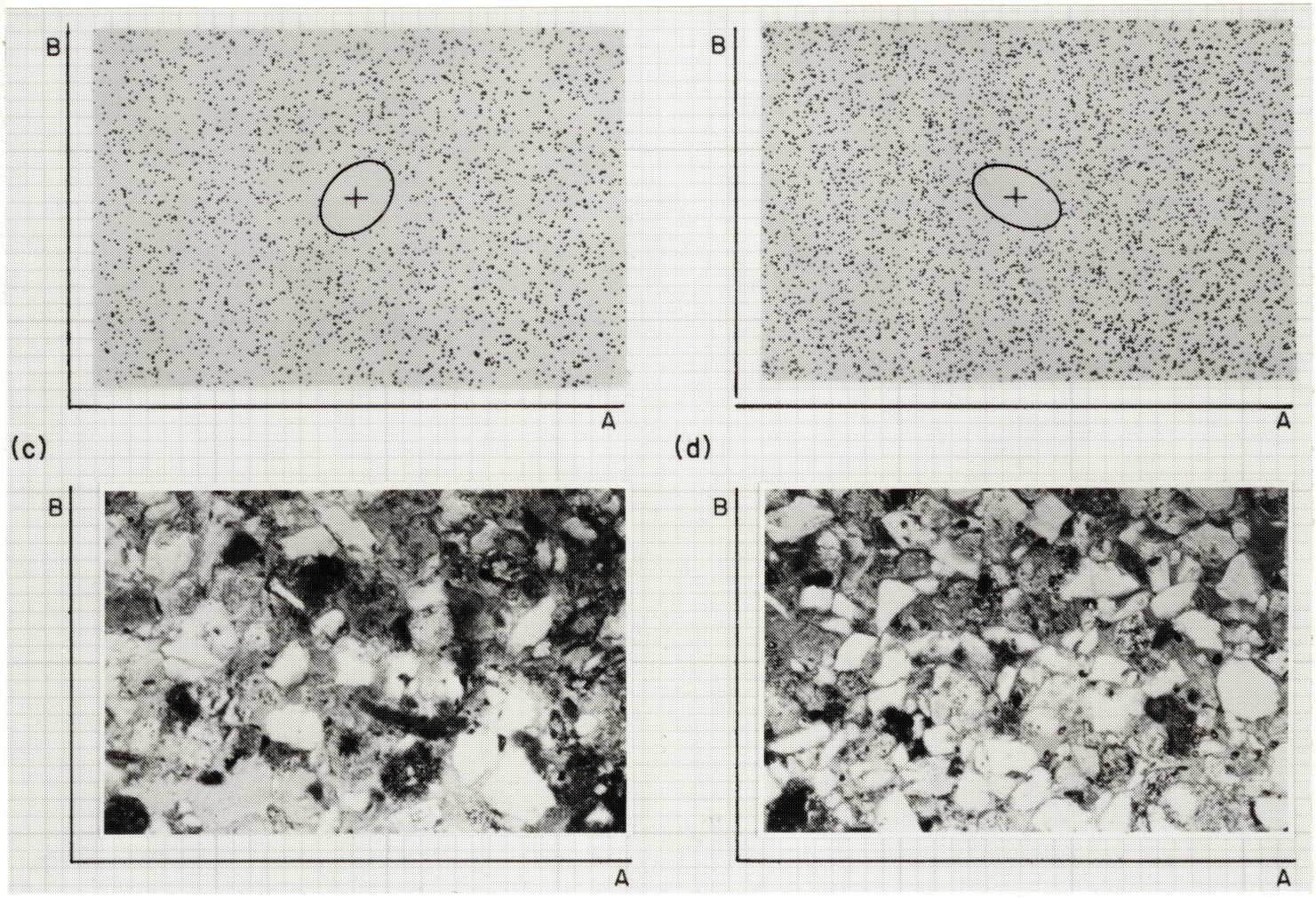


Figure 21 (cont.)

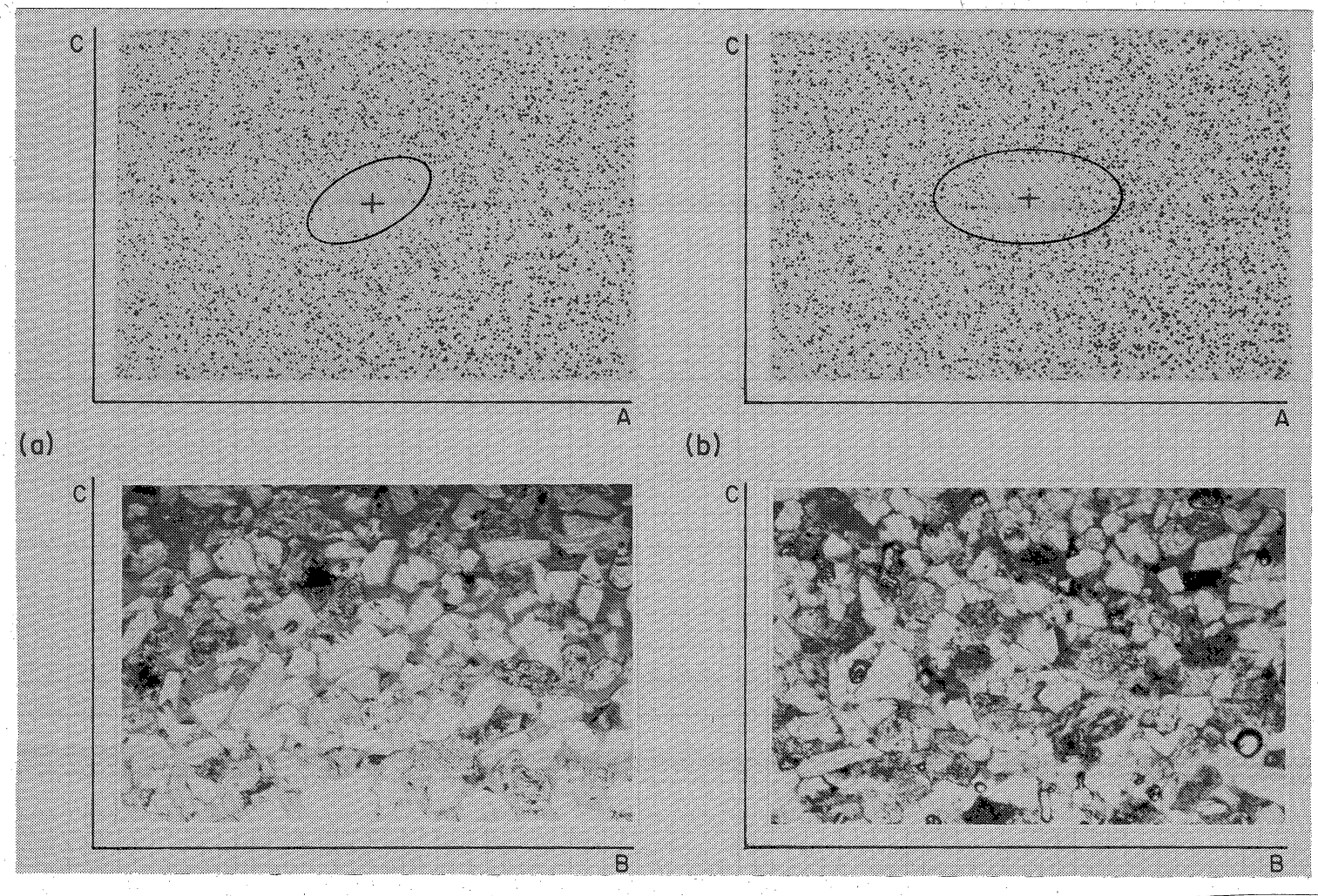


Figure 22. Fry (1979) diagrams for uncompacted (22a and 22c) and experimentally compacted (22b and 22d) Frio 'A' sandstones at 9,189.5 ft (2,801 m) with underlying plates showing grain fabric. The initial strain ellipse is imbricated with respect to bedding in vertical sections (22a). The greatest reduction in ellipse elongation from experimental compaction occurs in the section subparallel to bedding (22d).

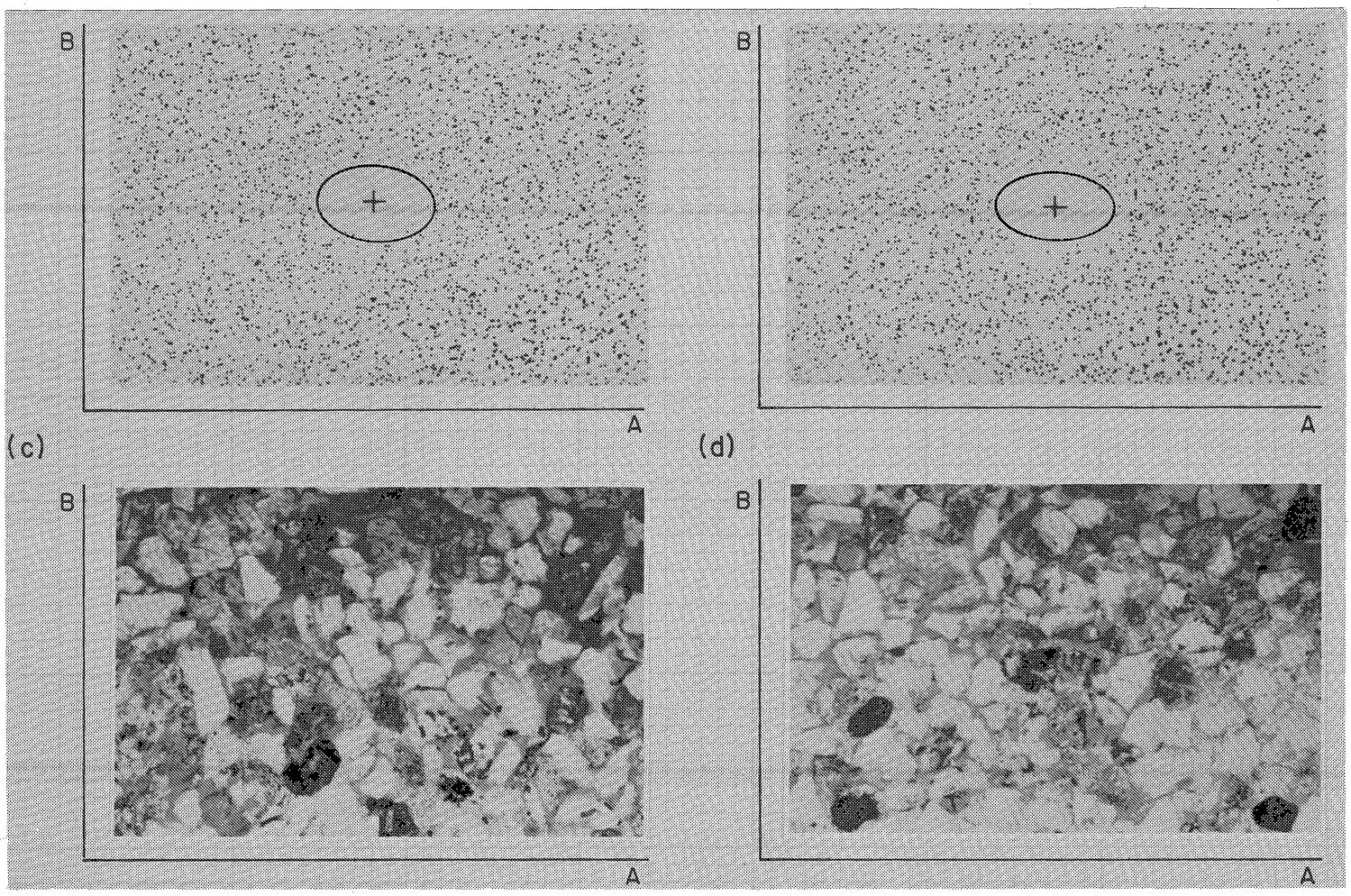


Figure 22 (cont.)

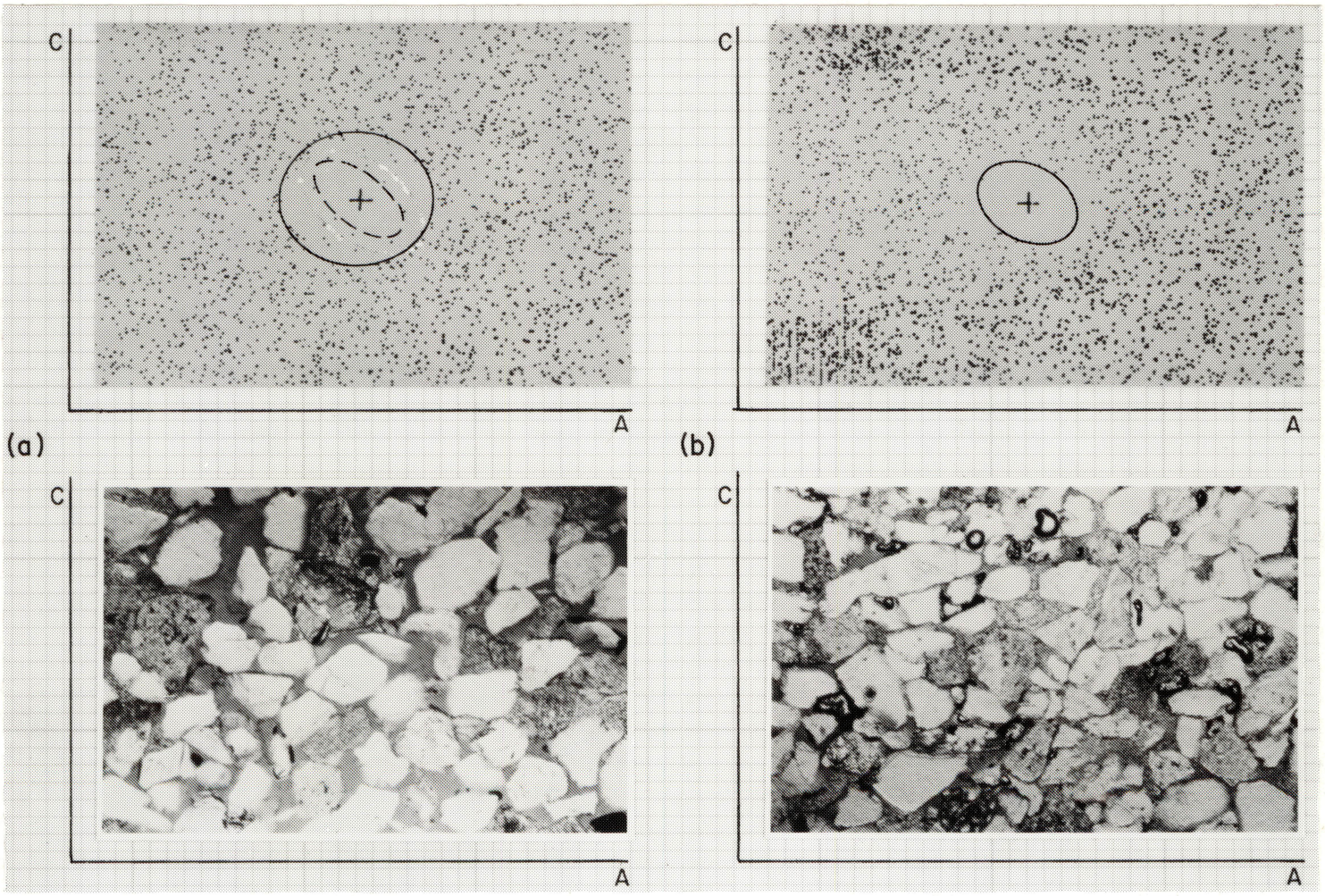


Figure 23. Fry (1979) diagrams for uncompacted (23a and 23c) and experimentally compacted (23b and 23d) Frio 'A' sandstones at 9,166 ft (2,794 m) with underlying plates showing grain fabric. The initial strain ellipse is imbricated with respect to bedding in vertical sections (23a) where the greatest reduction in ellipse elongation from experimental compaction is evident (23b).

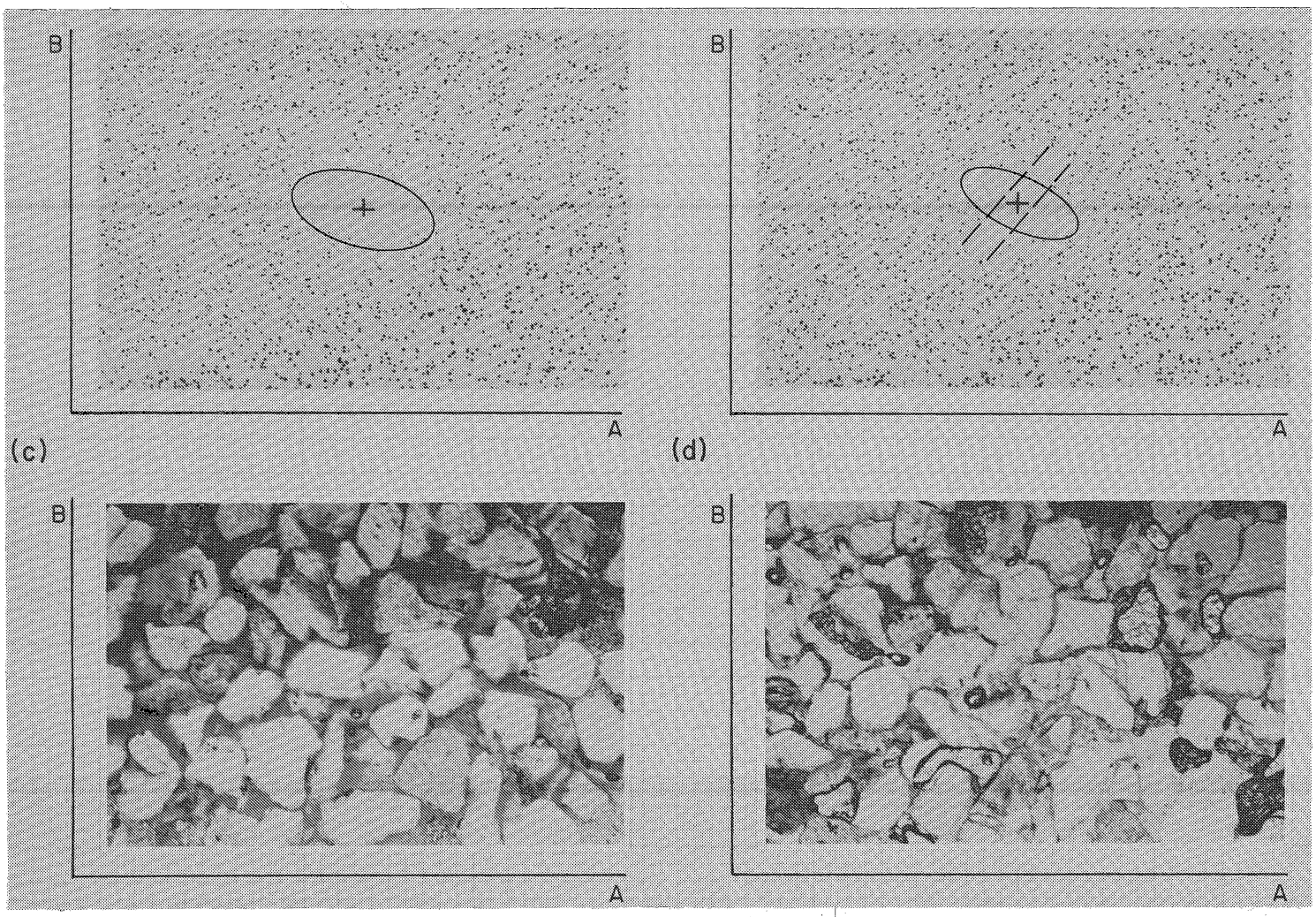


Figure 23 (cont.)

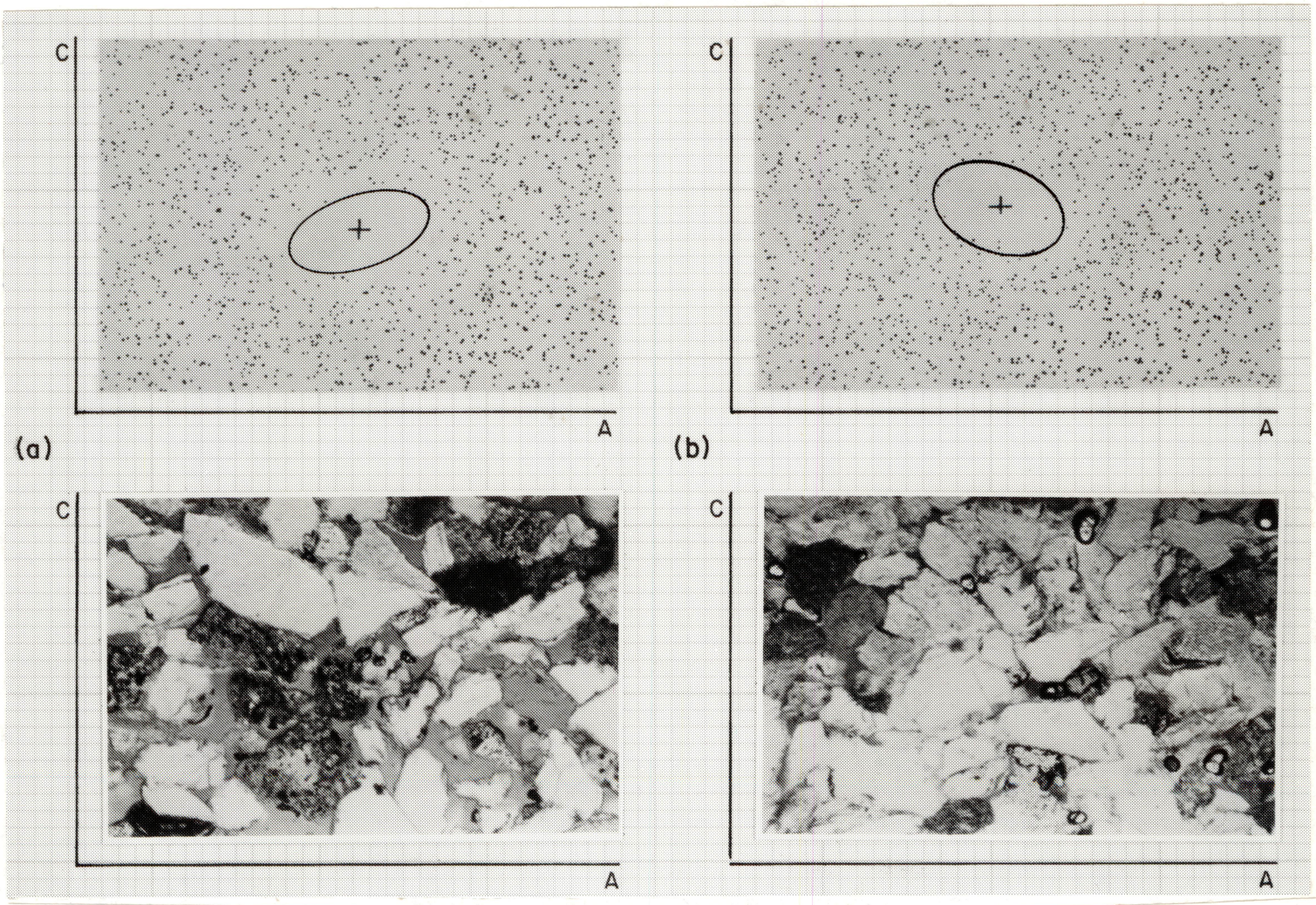


Figure 24. Fry (1979) diagrams for uncompacted Frio 'A' sandstones (24a and 24c)(9,178.3 ft, 2,797.6 m) and experimentally compacted Frio 'A' sandstones (24b and 24d)(9,177.5 ft, 2,797.3 m). Underlying plates show grain fabric. The initial strain ellipse is imbricated with respect to bedding in vertical sections (24a). The greatest reduction in ellipse elongation from experimental compaction occurs in the section subparallel to bedding (24d).

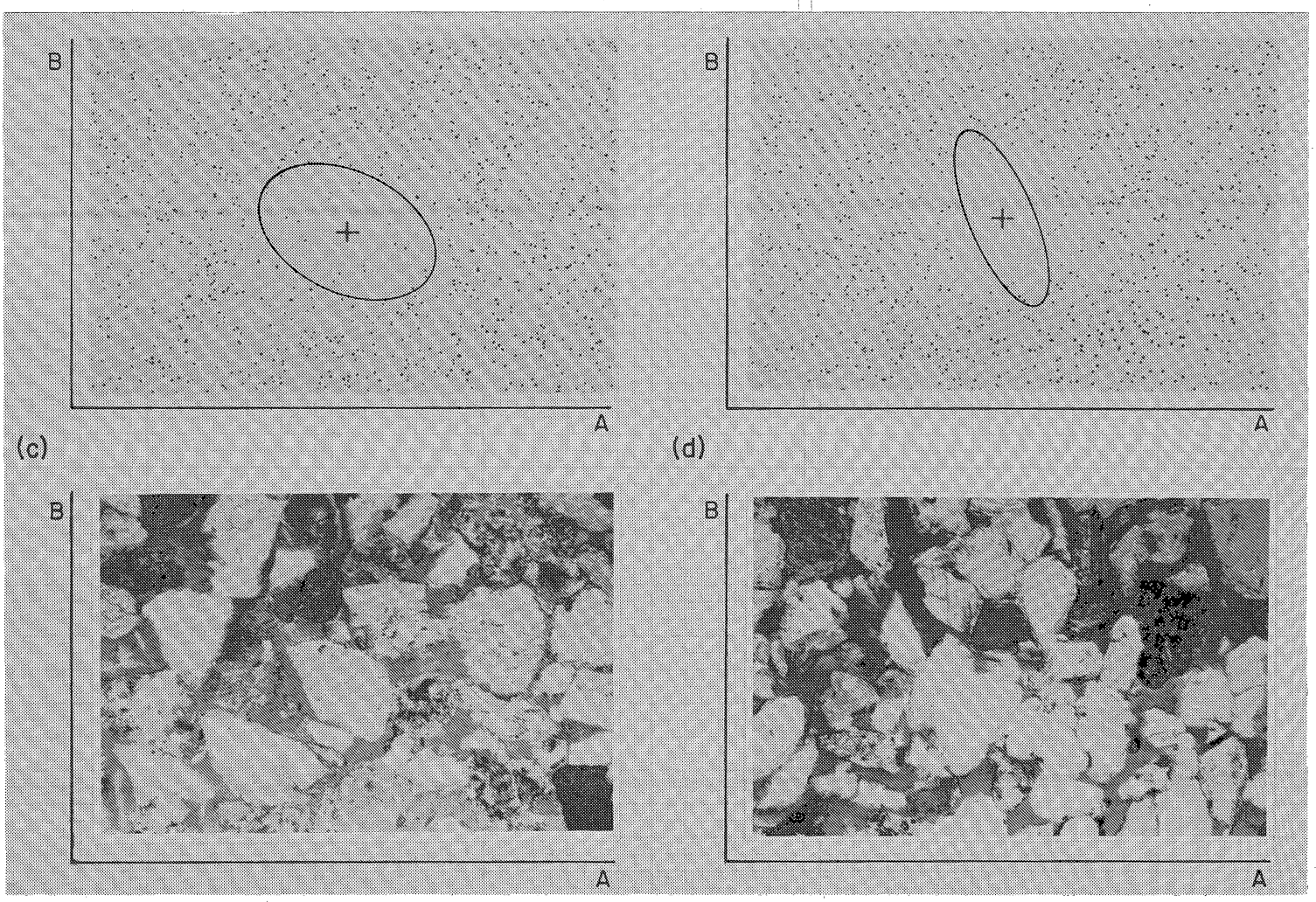


Figure 24 (cont.)

axial ratio of the vertical strain ellipse and increase the axial ratio of the horizontal strain ellipse, consistent with the interpretation from interference patterns. Reorientation of the grains into the bedding plane would be facilitated by the large amount of intergranular ductile materials and carbonate cements (26.4 percent, table 4) in the channel sandstone at 9,156 ft (2,791 m).

Well-developed initial strain ellipses are present in the vertical (fig. 22a) Fry (1979) diagrams (50 and 204 grain centers) of the cleaner, well-bedded channel sandstones at 9,189.5 ft (2,801 m). These strain ellipses have axial ratios of 2.9 and 1.9, respectively, whereas the strain ellipse in the vertical section is imbricated with respect to bedding. A similar well-developed strain ellipse is present in the Fry (1979) diagram generated from compacted sandstone (fig. 22b). Abundant noise in the vacancy field in the vertical Fry (1979) diagram (closely spaced grain centers) results from the comminution of grains, as already evidenced by rock flour in the sandstone. Strain ellipses are better developed with fewer grain centers (50; axial ratio 2.9) than they are with large numbers of grain centers (201; axial ratio 1.6) (fig. 22c) in Fry (1979) diagrams for horizontal sections. In these sections the strain ellipse is elongated perpendicular to the interference banding. The strain ellipse for a vertical section in the experimentally compacted sandstone at 9,189.5 ft (2,801 m) (204 grain centers) has increased by 13 percent to 2.1 (table 3, fig. 22b) and rotated through 40° to the horizontal (figs. 12 and 22b), while in the horizontal section (208 grain centers) it has been increased by 10.4 percent to 1.8 (table 4, fig. 22d). Evidently grain rotation in a vertical plane was accomplished by rotation and movement of grains into pore spaces in the bedding that resulted in a close packed structure, a circular strain ellipse in the bedding plane, and the greatest total shortening (12.1 percent, table 2).

An initial strain ellipse imbricated with respect to bedding is well developed in the vertical (axial ratio 2) (fig. 23a) Fry (1979) diagrams for the friable crossbedded bar sandstones at 9,166 ft (2,794 m). This ellipse is surrounded by an almost circular strain ellipse with an axial ratio of 1.1 in the Fry (1979) diagram generated with 214 grain centers. Evidently the circular strain ellipse represents the true state of strain of the uncompacted sandstone, whereas the elongated strain ellipse (for fewer grain centers) is a result of imbricated elongated grains. However the axial ratio of the initial strain ellipse in vertical sections (1.1, table 3, fig. 23a) is smaller than in the horizontal section (1.9, table 4, fig. 23c), so the imbricated grains appear better oriented in the bedding section. After experimental compaction, the axial ratio of the strain ellipse in the bar sandstones at 9,166 ft (2,794 m) has been increased by 14 percent to 1.3 in the vertical Fry (1979) diagram (table 3, fig. 23b), though it remains parallel to the imbricate direction. In a horizontal plane, compaction has reduced the axial ratio of the strain ellipse by 27 percent (table 4, fig. 23d) but it remains perpendicular to an interference banding. Most of the grain rotation and movement has occurred in the vertical plane into pore spaces within the bedding and produced the more closely packed structure (fig. 13, table 4).

The highly indurated crossbedded bar sandstones at 9,178.3 ft (2,797.6 m) have a well-developed initial strain ellipse imbricated with respect to bedding in vertical Fry diagrams using 50 grain centers (fig. 24a). The strain ellipse is poorly defined and subparallel to bedding when 187 grain centers are used to generate a Fry (1979) diagram (axial ratio 1.9, fig. 24a). In horizontal sections the strain ellipse is perpendicular to a grain layering but is also poorly defined (axial ratio 1.5, fig. 24c, table 3). The strain ellipse remains parallel to imbrication in a vertical section in Fry (1979) diagrams constructed with 50 and 193 grain centers in the compacted bar

sandstone at 9,178.3 ft (2,797.6 m) (fig. 24b). Experimental compaction has resulted in the axial ratio of the strain ellipse of the vertical section of the bar sandstone at 9,177.5 ft being decreased by 21 percent to 1.5 (table 3, fig. 24b), while the horizontal strain ellipse has been increased by 77 percent to 2.8 (table 4, fig. 24d). Grains have been rotated and moved into pore spaces within the bedding which resulted in a major change in the elongation of the strain ellipse and a more closely packed structure. This interpretation is consistent with the interference pattern data (tables 3 and 4).

## Compaction Modification of Fluid Flow Direction

Relatively clean distributary channel and mouth-bar sandstones (9,189.5 ft, 2,801 m; 9,166 ft, 2,794 m) show well-developed initial strain ellipses whose long axes are oriented parallel to normal imbrication. This preferred direction of grain orientation and porosity development will represent the preferential fluid-flow direction. As this orientation is oblique to both the foresets and the sedimentation unit boundaries (figs. 3, 17c, 17d, and 18) (Potter and Pettijohn, 1977), it allows easy movement of the fluids through the bedding interfaces. This interbed flow characteristic is preserved in the friable and highly indurated mouth-bar sandstones (9,166 ft, 2,793.8 m; 9,177.5 ft, 2,797.3 m) after experimental compaction because the strain ellipse remains parallel to the imbricate trend (figs. 23 and 24). The imbricate and foreset oriented grains in these sandstones have been rotated and moved into extension and shear fractures developed during compaction.

The initial strain ellipse parallels crossbeds (204 grain centers) and bedding (50 grain centers) in a vertical section through the uncompacted channel sandstone at 9,156 ft (2,791 m). The initial strain ellipse in a vertical section has a higher axial ratio than the initial strain ellipse for a horizontal section, which suggests that grain elongation, porosity development, and preferential fluid flow also run parallel to bedding (figs. 21a and 21c).

Compaction has rotated imbricated grains toward bedding in the clean distributary-channel sandstones (9,189.5 ft; 2,801 m) and (9,156 ft; 2,791 m). Here strain ellipsoid and preferential flow direction have become oriented subparallel to bedding, which greatly reduces the crossbed flow characteristics of these rocks, which show low porosities (7 to 8.5 percent) (fig. 12, table 1). Evidently interbed permeability is greatly reduced by compaction in the distributary-channel sandstones.

## MACROSCOPIC INTERPRETATION OF STRUCTURAL DATA

Porosity is reduced by 42 percent during experimental compaction in the clean, medium-grained, better sorted distributary-mouth-bar sandstones (9,166 ft, 2,794 m), which contain 13 to 19 percent of ductile grains and cements. In these rocks, incipient shear planes have developed and are surrounded by a zone of relatively uncompacted sandstone that retains almost the primary in-situ porosity (tables 1 and 2). Channel sandstones at 9,189.5 ft (2,801 m), which tend to be more poorly sorted, contain up to 26 percent of ductile grains, and cements show increased porosity reduction (62 percent) as well as shear formation (tables 1 and 2). Hence the cleaner sandstones not only will start with higher initial porosities but also will retain this porosity for a longer time during the pressure-drawdown-induced compaction. This is because sets of crosscutting shear planes with rimming high-porosity and high-

permeability zones will probably develop in the clean sandstones. In the dirtier sandstones porosity loss is faster and more homogeneous.

Permeability reduction can be estimated if the porosity and residual water saturation are known (fig. 25)(Timur, 1968). Porosities and permeabilities measured by conventional core analysis (Core Laboratories Inc., 1984) for Frio 'A' sandstones from the Delee No. 1 well and "point count" porosities for uncompacted and compacted sandstones are plotted on a Timur (1968) diagram. From these relationships the residual water saturations can be estimated at the four depths where compaction ("point count") porosity data are available (fig. 25).

"Point count" porosities are less than conventional porosities consistent with the findings of Loucks and others (1980) for Frio sandstones at the Pleasant Bayou well. Conventional porosity measurement in core plugs quantifies the total porosity but does not distinguish microporosity (pore throat diameter less than 1 $\mu$m) from macroporosity (pore throat diameter greater than 1$\mu$m) (Loucks and others, 1980). In the Pleasant Bayou well, conventional porosity does not correlate well with corresponding permeability measurements, whereas the effective macroporosity can be readily identified in thin sections (Loucks and others, 1980). Hence the determination of permeability from porosity requires the use of macroporosity alone, particularly where petrophysical logs are used (Loucks and others, 1980).

"Point count" porosities for the four sets of sandstones measured before and after experimental compaction were used to estimate the relative reduction in permeability (fig. 25). Although the "point count" porosity estimates are lower than

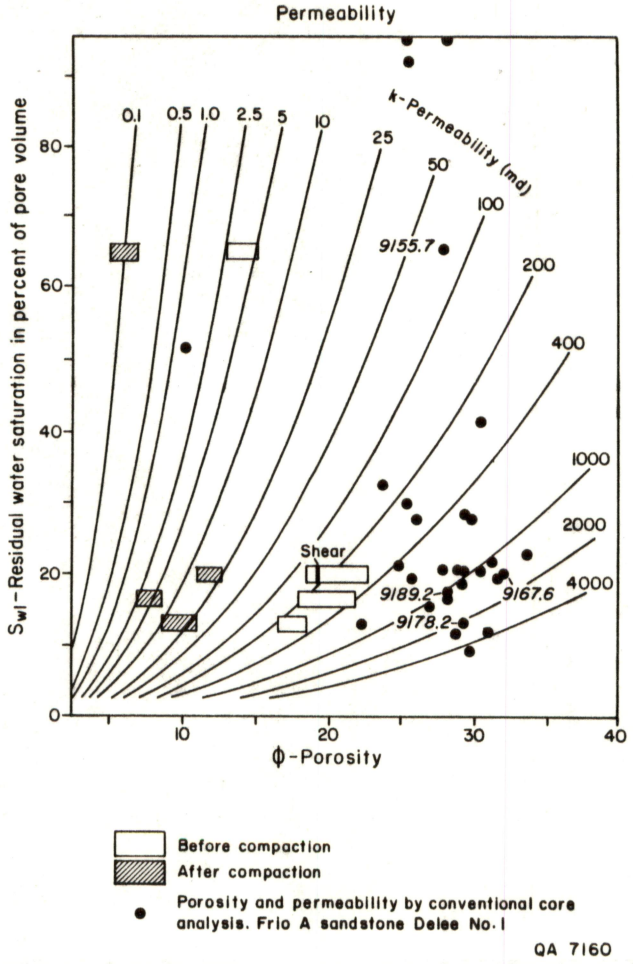


Figure 25. Estimated permeability reduction in Frio 'A' sandstones as a result of experimental compaction. Conventional core analysis data from Core Laboratories Inc. (1984). Residual water saturation versus porosity and permeability from Timur (1968).

the conventional porosities, the changes in permeability are probably meaningful. Permeability in the clean distributary-mouth-bar sandstones is reduced by 1/14 to 1/18 of the uncompacted values, while the dirtier channel sandstones have permeabilities reduced by 1/40 to 1/70 (fig. 25). The dirtier channel sandstones will tend to form increasingly effective vertical permeability barriers as pressure-drawdown-induced compaction proceeds (figs. 26a and 26b).

Steeply inclined compaction shear fractures should develop in both the clean and dirty sandstones and form effective conduits for the migration of fluids toward the well bore (fig. 26b). Shear fractures developed in the clean distributary mouth bar sandstones may have a rim zone of relatively uncompacted sandstone which with the fracture will act as a conduit guiding fluids from a compaction and pressure drawdown front to the well bore (fig. 26b). These shears should also propagate down through the tighter channel sandstones, thus retaining part of the vertical continuity of the producing formation (fig. 26b).

The in situ stress field in the Gulf Coast (greatest vertical stress sigma 1, least stress sigma 3, perpendicular to shore) has resulted in the predominance of listric growth faults. Decrease in fluid pressure (Pf) during production increases the magnitude of the greatest effective stress (sigma 1), but not the orientation of the stress field. We can therefore assume that the preferential orientation of compaction shears developed in the reservoir will mimic the trend of the growth fault systems (fig. 27). The compactional shear fractures should be subparallel to the long axes of fault blocks and dip at steep angles to the coast, except in areas of rollover where dips may be reversed. During production it is likely that the fracture sets will propagate outward as the pressure drawdown pulse and compaction front advances out from the well bore (figs. 27 and 28).

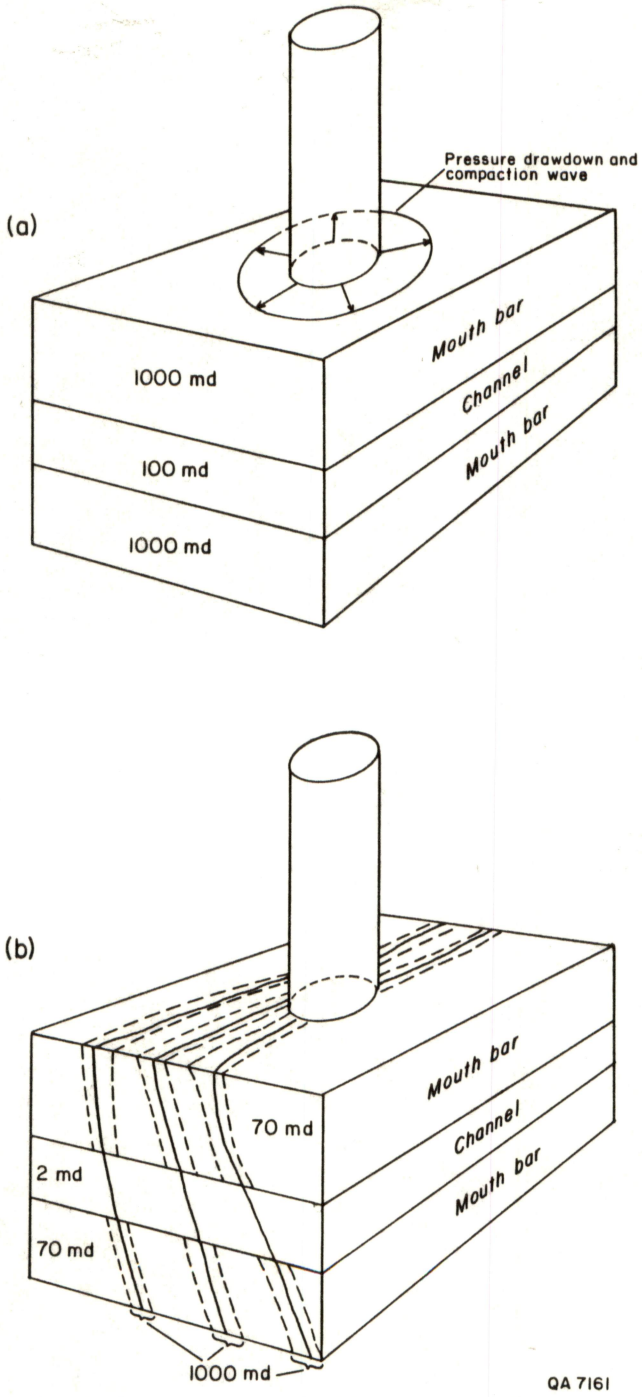


Figure 26. Hypothetical permeability distribution in mouth-bar and channel sandstones before (26a) and after (26b) production induced compaction and crosscutting shear formation. Permeabilities taken from figure 25.

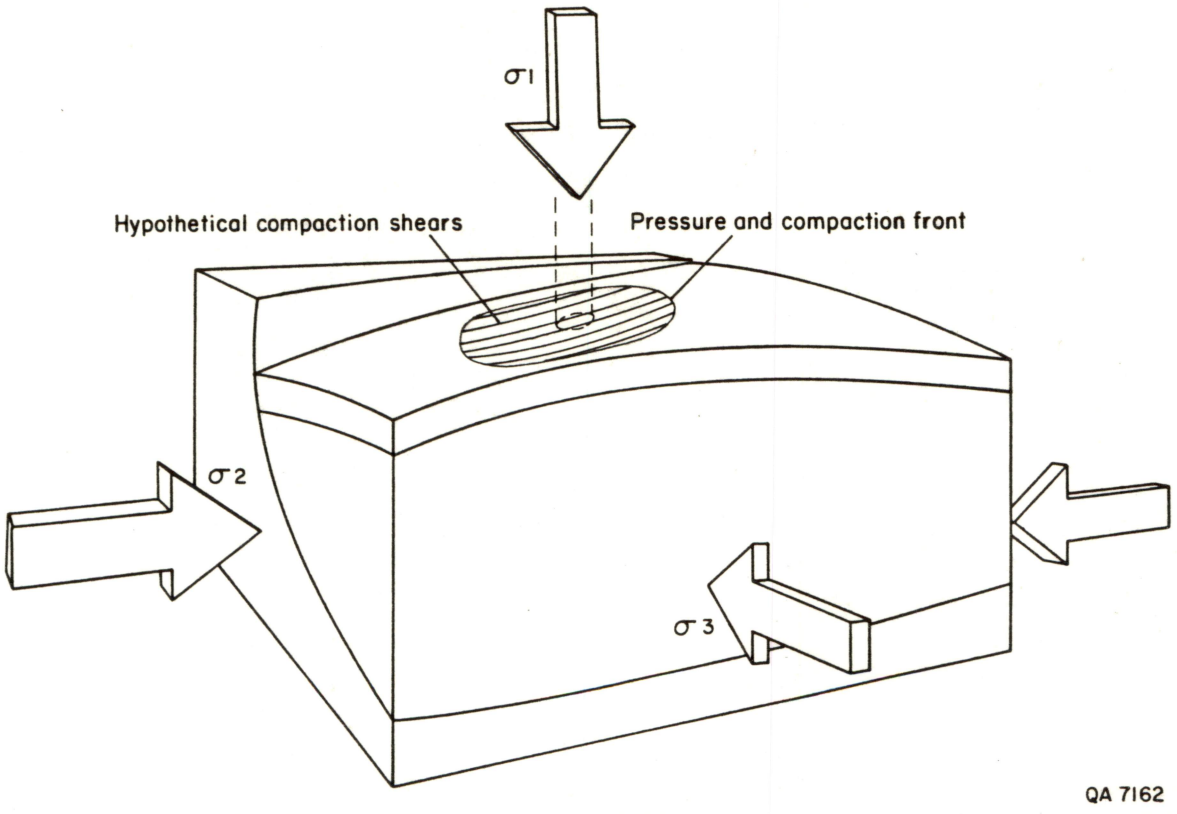


Figure 27. Hypothetical early development of compaction shears from the radial expansion of a pressure drawdown/compaction front during production from a geopressured or coproduction well.

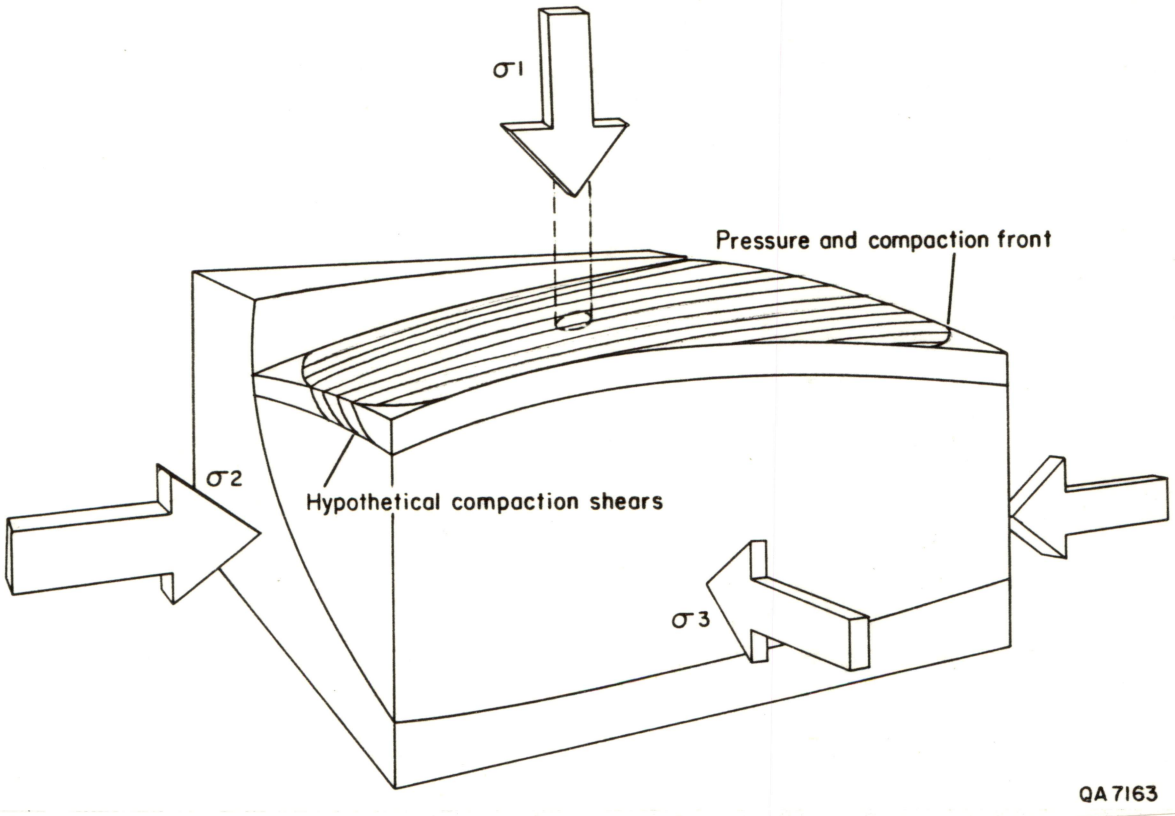


Figure 28. Hypothetical late development of compaction shears from the radial expansion of a pressure drawdown/compaction front during production from a geopressured or coproduction well. Compaction shears will probably subparallel growth fault systems.

## HYDRAULIC FRACTURING

Hydraulic fracturing has been extensively investigated as a method of stimulating geothermal reservoirs (Republic Geothermal Inc., 1980). To hydrostatically fracture subsurface formations, the hydraulic injection pressures should nearly equal the least principal stress (sigma 3), and the fracture occurs in a plane perpendicular to the least principal stress (Hubbert and Willis, 1957). There is little certainty about predicting fracture orientations and geometry although most fractures in deep wells are vertical (Haimson and Fairhurst, 1969).

Under normal conditions the greatest stress (sigma 1) is vertical and equal to the effective pressure of the overburden. The least stress (sigma 3) is horizontal and equal to 1/3 to 1/2 of the effective pressure of the overburden (Hubbert and Willis, 1957).

$$\text{Sigma 1} = Po - Pf$$

$$\text{Sigma 3} = 1/3 \text{ or } 1/2 \text{ Sigma 1}$$

Where:

Sigma 1 = effective vertical stress

Sigma 3 = least horizontal stress

Po = overburden pressure

Pf = fluid pressure

(Hubbert and Willis, 1957)

The in situ stress field along the Gulf Coast has resulted in predominantly down-to-the-coast listric growth faults, indicating that the least horizontal stress is oriented

perpendicular to the coastline. Hydraulic fractures developed in the deep subsurface should parallel the growth fault trend and natural shear fractures formed by increased compaction, which results from pressure drawdown during geopressured production. These compaction fractures may preferentially open during hydraulic fracturing, and because of their probable wide lateral extent parallel to growth fault systems, should form excellent conduits for fluid flow to the well bore.

## SEDIMENTOLOGICAL INTERPRETATION

Results of this structural analysis indicate that the Fry (1979) method can be used to define the initial fabric of poorly sorted, very porous sandstones that contain abundant elongated subangular grains because the Fry method only considers the average relationships of grain centers to one another (Fry, 1979). Besides allowing the estimation of the initial strain ellipse and axial ratio of a clastic aggregate (Fry, 1979; Lisle, 1979), this fabric analysis method can be used to accentuate more poorly developed packing fabrics. As already demonstrated, rhombic or square interference patterns defined by concentrations of points around the central vacancy field (Fry, 1979) probably result from open packed and more close packed fabrics, respectively (fig. 16). In other bar sandstones (9,166 ft, 2,794 m) interference bands inclined at 45 degrees to the horizontal define foresets within which the strain ellipse is imbricated at some 25 degrees to the boundary of the main sedimentation unit (fig. 17c and 17d). Consecutive layers with different packing fabrics should produce interference patterns on Fry (1979) diagrams which mimic the layering and show the type of packing present (fig. 17b). The more constant flow direction within rivers probably results in grains being more strongly imbricated and oriented within bedding parallel to flow in well bedded clean channel sandstones (fig. 22a) than in distributary-bar

sandstones (fig. 22b).

The existence of a strong fabric anisotropy in bedding sections in clastic sediments, a result of the combination of oriented elongate grains and porosity development can be used to define the trend of preferential fluid flow in sandstones (figs. 21c, 22c, 23c, and 24c). Where oriented cores are available in a sand body, the measured trend of the long axis of the strain ellipse on Fry (1979) diagrams can be used to regionally define high production-drainage and water-influx conduits. In addition the genesis or configuration of the sand body can be predicted when one of these parameters and the three-dimensional orientation of the sand grains (Reineck and Singh, 1975)(initial strain ellipsoid) are known.

Knowledge of the preferential fluid-flow directions in sandstone reservoirs is critical in efficiently locating production boreholes in geopressured and hydrocarbon reservoirs and guard wells in coproduction fields.

## CONCLUSIONS

Experimental compaction has reduced the porosity in the Frio 'A' channel and distributary-mouth-bar sandstones by 42 to 62 percent. Evidently, therefore, the major deformational mechanism in these rocks is intergranular slip, which allows grains to rotate and migrate into vacant pore spaces. The linear relationship that exists between percent porosity reduction and content of ductile grains and cements indicates that greater degrees of relative shortening have occurred where the ductile materials are abundant. These ductile grains and cements have deformed and lubricated grain

margins and facilitated intergranular rotation and movement. Collapse of vacuolized and skeletal feldspars, which represent about 2 percent of the sandstone volume, would only reduce the measured porosity by 7 to 10 percent.

Recognition of interference patterns on Fry (1979) diagrams, a result of packing arrangements and foreset bedding in Frio 'A' sandstones, implies that other diffuse sedimentary structures may be enhanced using the Fry method. Initial strain ellipses on Fry (1979) diagrams from Frio 'A' sandstones represent the preferred direction of grain orientation, porosity development, and fluid-flow direction. The effective location of production boreholes in geopressured and hydrocarbon reservoirs and guard wells in coproduction fields is largely controlled by knowledge of preferential fluid-flow directions.

Experimental compaction of channel sandstones has greatly diminished their cross-bed flow characteristics by reducing porosity and rotating the strain ellipsoid into bedding. In contrast, the clean distributary-mouth-bar sandstones have retained much of their crossbed flow characteristics as the strain ellipsoids have remained parallel to imbricate and shear directions.

Experimental compaction has rotated steeply dipping elongate imbricate grains into shear and extension fracture directions while more shallowly dipping grains have been rotated into bedding. Steeply inclined grains have been forced through bedding surfaces into vacant pore spaces to produce a closely packed fabric.

Clean distributary-mouth-bar sandstones show the preferential development of crosscutting compaction shears that are surrounded by a zone 3- to 5-mm wide, in which the precompaction porosity has been mostly preserved. During the large pressure drawdowns that result from high production rates in geopressured and co-

production reservoirs, compaction shears may develop and propagate out from the well bore as the pressure and compaction pulse migrate laterally into the formation. These fractures will form conduits for the migration of fluids through the compacted sandstones to the producing well. Hydraulic fracturing of the compacted sandstones should preferentially open these compaction fractures, increasing their conductivity.

## ACKNOWLEDGMENTS

Funding for this research was provided by the U.S. Department of Energy, Division of Geothermal Energy, under Contract No. DE-FC07-85NV10412. I thank M. P. A. Jackson, R. R. Cornelius, and S. E. Laubach for valuable discussions and assistance during data gathering. I am greatly indebted to R. W. Baumgardner and S. E. Laubach for instruction on the use of the program ROSEDIA and the computerized Fry method and to Ethel E. Butler for cutting excellent rock sections. Word processing was by Rosanne M. Wilson, under the direction of Lucille C. Harrell. Illustrations were drafted by Nan Minchow-Newman and Donald W. Thompson under the direction of Richard L. Dillon.

# REFERENCES

Bhattacharyya, T., and Longiaru, S., 1986, Ability of the Fry method to characterize pressure-solution deformation-discussion: Tectonophysics, v. 131, p. 199-200.

Blatt, H., Middleton, G., and Murray, R., 1972, Origin of sedimentary rocks: New Jersey, Prentice Hall, 634 p.

Coleman, J. M., and Prior, D. B., 1980, Deltaic sand bodies: American Association of Petroleum Geologists Education Course Note Series no. 15, 171 p.

Core Laboratories Inc., 1984, Core analysis report for Eaton Operating Co., Inc. No. 2 Louise, Hitchcock Field, Galveston County, Texas: Internal report, 11 p.

Crespi, J. M., 1986, Some guidelines for the practical application of Fry's method of strain analysis: Journal of Structural Geology, v. 8, no. 7, p. 799-808.

Curray, J. R., 1956, Dimensional grain orientation studies of recent coastal sands: American Association of Petroleum Geologists Bulletin v. 40, p. 2440-2456.

Fry, N., 1979, Random point distributions and strain measurement in rocks: Tectonophysics, v. 60, p. 89-105.

Haimson, B., and Fairhurst, C., 1969, Hydraulic fracturing in porous-permeable materials: Journal of Petroleum Technology, p. 811-817.

Hanna, S. S., and Fry, N., 1979, A comparison of methods of strain determination in rocks from southwest Dyfed (Pembrokeshire) and adjacent areas: Journal of Structural Geology, v. 1, p. 155-162.

Hubbert, M. K., and Willis, D. G., 1957, Mechanics of hydraulic fracturing: Journal of Petroleum Technology, v. 210, p. 153-168.

Kaiser, W. R., and Richmann, D. L., 1981, Predicting diagenetic history and reservoir quality in the Frio Formation of Brazoria County, Texas, and Pleasant Bayou test wells, in Proceedings, fifth conference on geopressured geothermal energy: The University of Texas at Austin, p. 67-74.

Light, M. P. R., 1985, Structure, facies, continuity, and internal properties of the Frio 'A' sandstone, N.E. Hitchcock field, Galveston County, Texas, in Dorfman, M. H., and Morton, R. A., (eds.), Geopressured-geothermal energy: New York, Pergamon, p. 229-238.

Light, M. P. R., and D'Attilio, W., 1985, Structure, facies, and internal properties of the Frio 'A' reservoir, Hitchcock, N. E., field, Galveston County, Texas, in Finley, R. J., Morton, R. A., Dorfman, M. H., and Sepehrnoori, K., Coordination of geological and engineering research in support of Gulf Coast co-production program: The University of Texas at Austin, Bureau of Economic Geology, report prepared for the Gas Research Institute, Contract No. 5084-212-0924, p. 1-51.

Lisle, R. J., 1979, Strain analysis using deformed pebbles; the influence of initial pebble shape: Tectonophysics, v. 60, p. 263-277.

Loucks, R. G., Richman, D. L., and Milliken, K. L., 1980, Factors controlling porosity and permeability in geopressured Frio sandstone reservoirs, General Crude Oil/Department of Energy Pleasant Bayou test wells, Brazoria County, Texas, in Proceedings, fourth conference on geopressured geothermal energy: The University of Texas at Austin, v. 1, p. 46-82.

McBride, E. F., 1960, Martinsburg flysch of the central Appalachians: The Johns Hopkins University, Ph.D. dissertation, 375 p.

Nachtigall, K. H., 1962, Uber die regelung von langquarzen in aquatisch sedimentierten sanden: Meyniana, v. 12, p. 9-24.

Nanz, R. H., 1955, Grain orientation in beach sands; a possible means for predicting reservoir trends (abs.): Journal of Sedimentary Petrology, v. 25, p. 130.

Onasch, C. M., 1986a, Ability of the Fry method to characterize pressure-solution deformation--reply: Tectonophysics, v. 122, p. 187-193.

_____ 1986b, Ability of the Fry method to characterize pressure-solution deformation--reply: Tectonophysics, v. 131, p. 201-203.

Potter, P. E., and Mast, R. F., 1963, Sedimentary structures, sand shape fabrics and permeability, part 1: Journal of Geology, v. 71, p. 548-565.

Potter, P. E., and Pettijohn, F. J., 1977, Paleocurrents and basin analysis: Berlin, Springer Verlag, 425 p.

Ragan, D. M., 1968, Structural geology, an introduction to geometrical techniques: New York, Wiley, 166 p.

Ramsay, J. G., and Huber, M. I., 1983, The techniques of modern structural geology, Volume 1: strain analysis; London, Academic Press, 307 p.

Reineck, H. E., and Singh, I. B., 1975, Depositional sedimentary environments: New York, Springer Verlag, 439 p.

Republic Geothermal Inc., 1980, Geothermal reservoir well stimulation program; technology transfer: Prepared by Maurer Engineering Inc. for the U.S. Department of Energy, Contract No. DE-AC32-79AL10563, v. IV, no. 2, 139 p.

Rousell, D. H., 1972, The Chelmsford formation of the Sudbury Basin - a Precambrian turbidite. Special Paper of the Geological Society of Canada, v. 10, p. 79-91.

Rusnak, G. A., 1957, The orientation of sand grains under condition of "unidirectional" fluid flow. 1. Theory and experiment: Journal of Geology, v. 65, p. 384-409.

Schwarzacher, W., 1951, Grain orientation in sands and sandstones: Journal of Sedimentary Petrology. v. 21, p. 162-172.

Seibold, E., 1963, Geological investigation of near-shore sand transport, in Sears, M., ed., Progress in oceanography: Oxford, Pergamon, v. 1, p. 1-70.

Selley, R. C., 1979, Concepts and methods subsurface facies analysis, sessions 7, 8, 9: Johannesburg, Republic of South Africa, Short course, 10 p.

Spiramadas, A., 1957, Appositional fabric study of the coastal sedimentaries, East Godawari district, Andhra, India: Journal of Sedimentary Petrology, v. 27, p. 447-452.

Timur, A., 1968, An investigation of permeability, porosity, and residual water saturation relationships for sandstone reservoirs: The Log Analyst, v. 9, no. 4, p. 8-17.

Turner, F. J., and Weiss, L. F., 1963, Structural analysis of metamorphic tectonites: New York, McGraw-Hill, 545 p.

Wanless, H. R., Belknap, R. L., and Foster, H., 1955, Paleozoic and Mesozoic rocks of the Gros Ventre, Teton, Holback, and Snake River ranges, Wyoming: Memoirs of the Geological Society of America, no. 63, 90 p.

Wendler, R., 1956, Zur frage der quarz-kornregelung von psammiten: Wiss. Z. Karl-Marx-University, Leipzig, v. 5, p. 421-426.

_____ 1961, Beziehungen zwischen fluidtexturen und der magnetischen anisotropie der gesteine: Notizbl. hess. Landesamtes Bodenforsch, v. 89, p. 420-437.

Young, L. M., and Mankin, C. J., 1961, Dimensional grain orientation studies of recent Canadian river sands: Oklahoma Geological Survey, Oklahoma Geological Notes, no. 21, p. 99-107.